Article

Developmental Cell

Metabolic plasticity drives development during mammalian embryogenesis

Graphical abstract

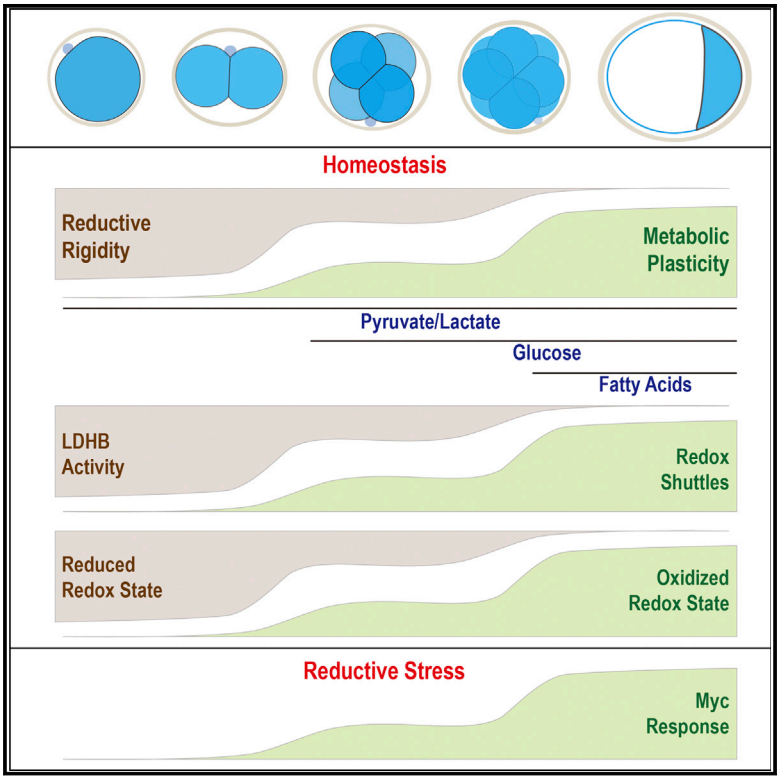

Highlights

- Metabolomic analysis of metabolic plasticity during preimplantation development
- Strong sensitivity to reductive stress in early embryos attenuates with maturity
- Changes in redox balance controls metabolic plasticity in later-stage embryos
- Myc reprograms embryonic glucose and glutamine metabolism to counter reductive stress

Authors

Mark S. Sharpley, Fangtao Chi, Johanna ten Hoeve, Utpal Banerjee

Correspondence

Mark.Sharpley@cshs.org (M.S.S.), banerjee@mbi.ucla.edu (U.B.)

In brief

Sharpley et al. investigate the metabolic reprogramming occurring during the earliest steps of mammalian development, the preimplantation period. They reveal the importance of redox state in regulating metabolic rigidity and plasticity at specific developmental steps and identify a role for Myc in mediating reprogramming of embryonic metabolism.

Sharpley et al., 2021, Developmental Cell *56*, 2329–2347
August 23, 2021
https://doi.org/10.1016/j.devcel.2021.07.020

CellPress

Developmental Cell

CellPress

Article

Metabolic plasticity drives development during mammalian embryogenesis

Mark S. Sharpley,[1,6,7,*] Fangtao Chi,[1,2,4,6] Johanna ten Hoeve,[5] and Utpal Banerjee[1,2,3,4,*]

[1]Department of Molecular, Cell and Developmental Biology, Los Angeles, CA 90095, USA
[2]Molecular Biology Institute, Los Angeles, CA 90095, USA
[3]Department of Biological Chemistry, Los Angeles, CA 90095, USA
[4]Eli and Edythe Broad Center of Regenerative Medicine and Stem Cell Research, Los Angeles, CA 90095, USA
[5]UCLA Metabolomics Center, Department of Molecular and Medical Pharmacology, University of California, Los Angeles, Los Angeles, CA 90095, USA
[6]These authors contributed equally
[7]Lead contact
*Correspondence: Mark.Sharpley@cshs.org (M.S.S.), banerjee@mbi.ucla.edu (U.B.)
https://doi.org/10.1016/j.devcel.2021.07.020

SUMMARY

Mammalian preimplantation embryos follow a stereotypic pattern of development from zygotes to blastocysts. Here, we use labeled nutrient isotopologue analysis of small numbers of embryos to track downstream metabolites. Combined with transcriptomic analysis, we assess the capacity of the embryo to reprogram its metabolism through development. Early embryonic metabolism is rigid in its nutrient requirements, sensitive to reductive stress and has a marked disequilibrium between two halves of the TCA cycle. Later, loss of maternal LDHB and transcription of zygotic products favors increased activity of bioenergetic shuttles, fatty-acid oxidation and equilibration of the TCA cycle. As metabolic plasticity peaks, blastocysts can develop without external nutrients. Normal developmental metabolism of the early embryo is distinct from cancer metabolism. However, similarities emerge upon reductive stress. Increased metabolic plasticity with maturation is due to changes in redox control mechanisms and to transcriptional reprogramming of later-stage embryos during homeostasis or upon adaptation to environmental changes.

INTRODUCTION

During mammalian preimplantation development, a single cell (1C), the zygote, develops into the blastocyst (Rossant, 2018). In mice, this process takes 4–5 days. The embryo relies on maternal proteins and mRNAs until the 2C stage (“2C stage embryo” is called just “2C” here for simplicity) when it activates its own genome (zygotic genome activation, ZGA). The embryo undergoes compaction at 8C (White et al., 2016), and differentiates into the TE (trophectoderm) and the ICM (inner cell mass) (Leung et al., 2016).

Decades of research has highlighted the important role of metabolism in preimplantation development (Biggers et al., 1967; Brinster, 1963; Leese, 2012). Pyruvate is indispensable for development beyond 2C (Figure 1A) and ZGA, following which either pyruvate or lactate can facilitate development (Brown and Whittingham, 1991; Lane and Gardner, 2005; Nagaraj et al., 2017), but unlike for cultured cancer cells or ESCs (Altman et al., 2016; Intlekofer and Finley, 2019; Liberti and Locasale, 2016; Pavlova and Thompson, 2016; Vander Heiden and DeBerardinis, 2017; Zhang et al., 2016) glucose or glutamine (Gln) are not able to do so. However, glucose becomes essential at 8C for the transition from morula to blastocysts (Brown and Whittingham, 1991; Chi et al., 2020; Martin and Leese, 1995).

Here, we present the first comprehensive stable isotope-resolved metabolomic analysis across all stages of preimplantation development and correlate these results with transcriptomic analysis to characterize the capacity of the embryo to reprogram its metabolism during normal development and in response to stress.

RESULTS

Glucose metabolism during preimplantation development

We traced the fate of ^{13}C labeled glucose to track labeled metabolites that result from its breakdown in the 2C, morula, and blastocyst stages. For all three sets of data, medium containing U^{13}C glucose (i.e., all six glucose carbons are labeled) is added at the zygote stage (time of isolation). For the first set, embryos are incubated until the 2C stage, and then metabolites are isolated for analysis. For the second set, fresh medium containing label is added when the zygote (1C) becomes 2C, these embryos are allowed to develop in the fresh labeled medium to the morula stage and are then analyzed for the distribution of glucose-derived ^{13}C. For the third set, the embryos are incubated in the original medium from 1C to morula, at which point fresh media containing labeled glucose is added. The embryos are further

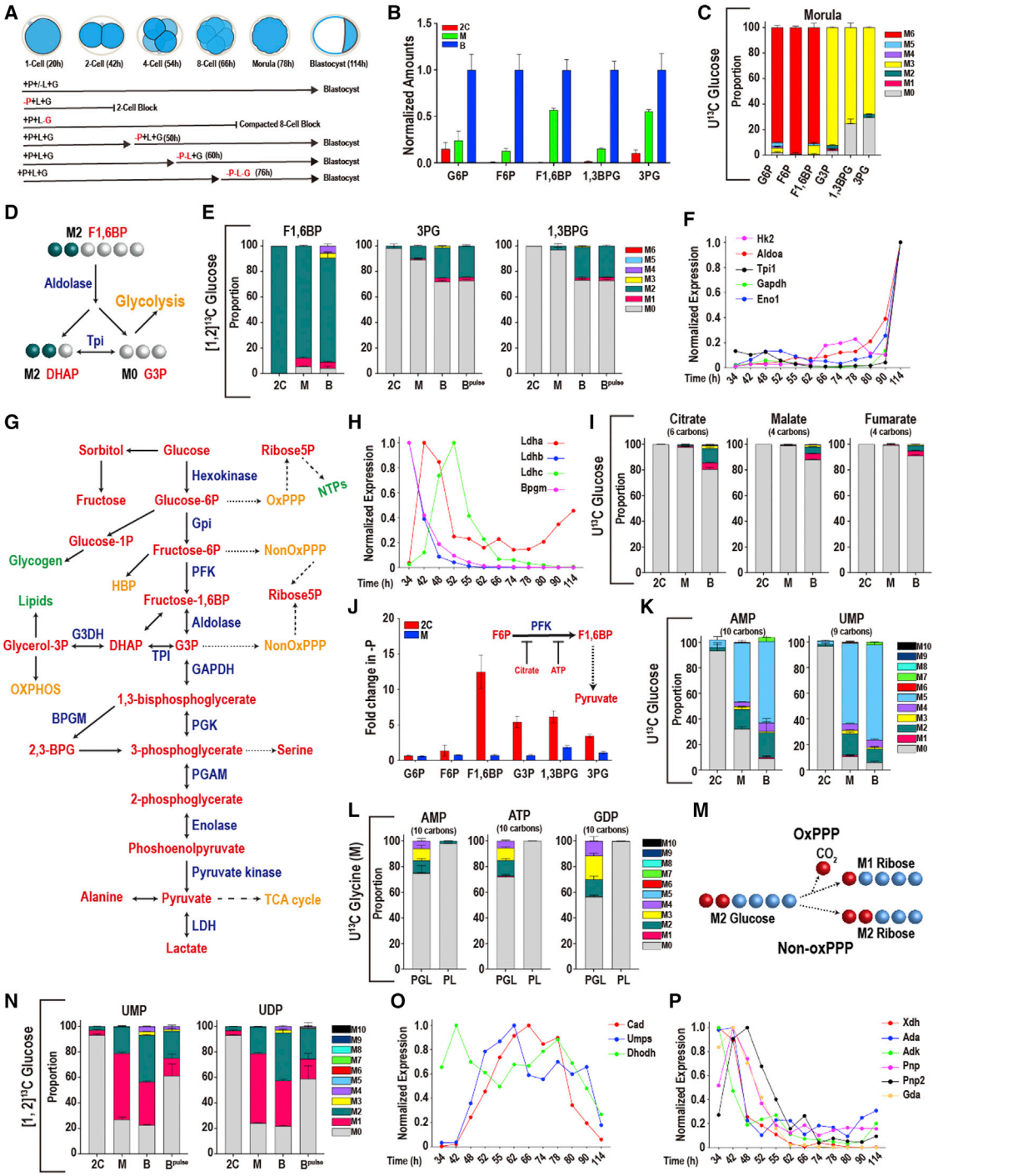

Figure 1. Glucose metabolism during preimplantation development

In this and in all figures, times in hours (h) refer to time elapsed after human chorionic gonadotropin (hCG) injection that induces ovulation. Zygotes are isolated at 18–22 h and cultured until the specified hours (h) post-hCG. The metabolomic analysis is presented as scaled means ± SD and is obtained from 3 biological replicates. Each biological replicate contains more than 250 embryos. The RNA-seq analysis is presented as normalized values and is obtained from ~4 biological replicates of each of the 12 time points that were analyzed. Each biological replicate contains RNA from 25 embryos.

(A) A schematic representation of developmental progression of mouse preimplantation embryos in the presence of different combinations of nutrients.

(B) Normalized amounts of glycolytic intermediates in 2C (48 h), morula (M, 78 h), and blastocysts (B, 96 h). See Table S1 for non-normalized data.

(C) U-^{13}C glucose contributes carbon to the glycolytic intermediates at the morula stage. The lower glycolytic intermediates (1,3BPG and 3PG) have a prominent unlabeled component (gray). Gray, M0 unlabeled; colors, labeled as marked. Note that the "fully labeled" color depends on the total carbons in the metabolite (e.g., fully labeled is M6 [red] for G6P, M3 [yellow] for 1,3BPG and 3PG).

(D) Schematic representing the fate of the 1 and 2 carbon of glucose at the aldolase reaction.

(legend continued on next page)

incubated to the blastocyst when metabolites are isolated and analyzed. In sum, regardless of the stage, the embryo sees a round of fresh media with labeled glucose for 26 h prior to metabolomic analysis.

A significant advantage of using ^{13}C labeling is that the breakdown of a nutrient can be traced by isotopologue analysis. Thus, if a 6-carbon target metabolite is fully labeled by U^{13}C glucose its mass will increase by 6 Da (the M6 isotopologue) (Buescher et al., 2015; Jang et al., 2018) (schematic in Figure S1A). Whereas, if a 5-carbon metabolite is fully labeled, its mass will increase by 5 Da (the M5 isotopologue). A fully unlabeled metabolite with ^{12}C only is M0.

The glycolytic intermediates are schematized in Figure 1G. Glycolytic intermediates increase in abundance from 2C to blastocyst (Figure 1B). In morulae and blastocysts, a majority of G6P, F6P, and F1,6BP (M6) are extensively labeled by U^{13}C glucose (Figures 1C and S1B), while the labeling of 1,3BPG and 3PG (M3) is partial (Figure 1C).

As an alternative assay, instead of U^{13}C, we use glucose that is only labeled at positions 1 and 2. In glycolysis, at the aldolase step, the 6-carbons from glucose are split into the two 3-carbon metabolites, DHAP (that receives both ^{13}Cs) and G3P (that receives none). In most systems, these two triose phosphates equilibrate rapidly such that the labels on DHAP are transmitted efficiently to G3P and to lower glycolysis (Figure 1D). This equilibration of the triose phosphate pool and a major transfer of DHAP carbons to lower glycolysis is not seen (Figure 1E). Labeling data also do not support oxPPP-derived carbons reentering glycolysis (Figure 1E).

Transcriptomic analysis shows that expression of glycolytic genes such as *Hk2*, *Aldoa*, *Gapdh*, *Tpi1*, *Eno1*, and glucose transporter *Slc2a3*, hardly detectable in cleavage-stage embryos, increases dramatically at the blastocyst stage (Figures 1F, S1C, and S1D). Genes related to glucose-linked bioenergetic status and not core glycolysis such as lactate dehydrogenase (*Ldhb*, *Ldhc*) and bisphosphoglycerate mutase (*Bpgm*) are much higher in early embryos than in the blastocyst (Figure 1H).

In 2C, morula, and blastocysts, glucose contributes minor amounts of carbon to acetyl-carnitine (reflecting the levels of acetyl-CoA), the TCA cycle metabolites and amino acids (Figures 1I and S1E–S1G). Given that there is lactate and pyruvate in the medium, exchange of any glucose-derived pyruvate with unlabeled lactate/pyruvate carbons is a contributing factor for the lack of TCA cycle labeling by glucose. In addition to exchange, low glucose uptake (Leese and Barton, 1984), the low expression of glucose transporters, and upper glycolytic enzymes at 2C lead to very low levels of lower glycolytic intermediates, which also contribute to a virtual absence of glucose-derived pyruvate driving the TCA cycle.

We compared metabolites from embryos grown with and without pyruvate from 1C to late 2C (Figure 1J). For a later-stage comparison, metabolites were extracted at the morula stage. Control embryos were grown with pyruvate until the morula stage and compared with embryos grown without pyruvate from late 2C. In the 2C comparison, pyruvate withdrawal does not affect G6P and F6P whereas the lower metabolites F1,6BP, G3P, 1,3BPG, and 3PG all increase. This is consistent with Lowry (Barbehenn et al., 1974). Interestingly, this increase is not seen in the morula (Figure 1J). Pyruvate is required to keep citrate and ATP levels high in 2C. Together, ATP and citrate inhibit the enzyme PFK, posing an additional impediment for the transmission of glucose carbons to the lower glycolytic intermediates. When pyruvate is removed, ATP and citrate levels fall in 2C (see later), relieving the block in PFK function.

Unlike for TCA cycle metabolites and amino acids, exogenous glucose plays an increasing role in populating nucleotides with its carbon. The contribution of added glucose to nucleotides is barely detectable at the 2-cell stage. In the blastocyst, nearly all the ribose carbons in nucleotides are derived from exogenously provided glucose (Figures 1K and S1H for scheme). Previous work (Brown and Whittingham, 1991; Chi et al., 2020; Martin and Leese, 1995) have shown that a pulse of glucose lasting only the 1C-2C stages fully rescues development. This 26-h period is too early for nucleotide synthesis. However, when "pulsed" embryos and those exposed continuously to glucose are analyzed for their isotopologue pattern of nucleotide labeling at the morula stage, the patterns are fairly similar (Figure S1J). Thus, glucose carbons added to the zygote are retained, perhaps as glycogen, for nucleotide synthesis at a later time when glucose from the media is no longer available to the embryo.

(E) [1, 2]-^{13}C glucose contributes carbon to the upper glycolytic intermediates (F1,6BP) at the 2C, morula (M), and blastocyst (B) stages. The lower glycolytic intermediates (1,3BPG and 3PG) are largely unlabeled, with an increased contribution at the blastocyst stage. For the blastocyst samples, labeled glucose is provided at the zygote stage (B) or 26 h prior to extraction (B^{pulse}). Colors: labeled as marked.
(F and H) Expression of genes encoding glycolytic enzymes between early 2C (34 h) and fully expanded blastocyst (114 h) stages.
(F) A majority of glycolytic enzymes increase in expression during later stages of development.
(H) A subset is highest at the 2C stage and then declines.
(G) Schematic of glucose metabolism. Red, metabolites; blue, enzymes; green, products; orange, pathways.
(I) U-^{13}C glucose only contributes minor amounts of carbon to TCA cycle metabolites, with a measurable contribution only at the blastocyst stage.
(J) The lower glycolytic intermediates (G3P, 1,3BPG, and 3PG) increase in abundance in 2C embryos following pyruvate withdrawal, but not in morula. Inset: schematic illustration of the inhibition of PFK activity by citrate and ATP.
(K) U-^{13}C glucose contributes to nucleotide formation during development. The major isotopologue, M5 (blue) represents fully labeled ribose formation by glucose.
(L) U-^{13}C glycine contributes to purine base synthesis in morulae (M) if glucose (U-12C) is present (PGL) but does not do so when glucose is withheld (PL).
(M) Schematic showing that when [1, 2]^{13}C glucose is metabolized by the oxidative PPP, one labeled carbon is lost to CO_2 formation and the ribose-5P formed is M1. When [1, 2]-13C glucose is metabolized by the non-oxidative PPP, a carbon is not lost and the ribose-5P formed is M2.
(N) [1, 2]^{13}C glucose contributes carbon to the pyrimidine nucleotides UMP and UDP at the morula (M) and blastocyst (B) stages. M1 (pink) indicates ribose formation by the oxidative PPP, and M2 (green) ribose formation via the non-oxidative PPP. For the blastocyst samples, labeled glucose is provided at the zygote stage (B) or 26 h prior to extraction (B^{pulse}).
(O and P) Expression of nucleotide metabolism genes. A majority of pyrimidine synthesis genes (O) increase in expression during the morula stage, whereas genes involved in purine degradation (P) peak in expression during the 2C stage.
See also Figure S1; Table S1.

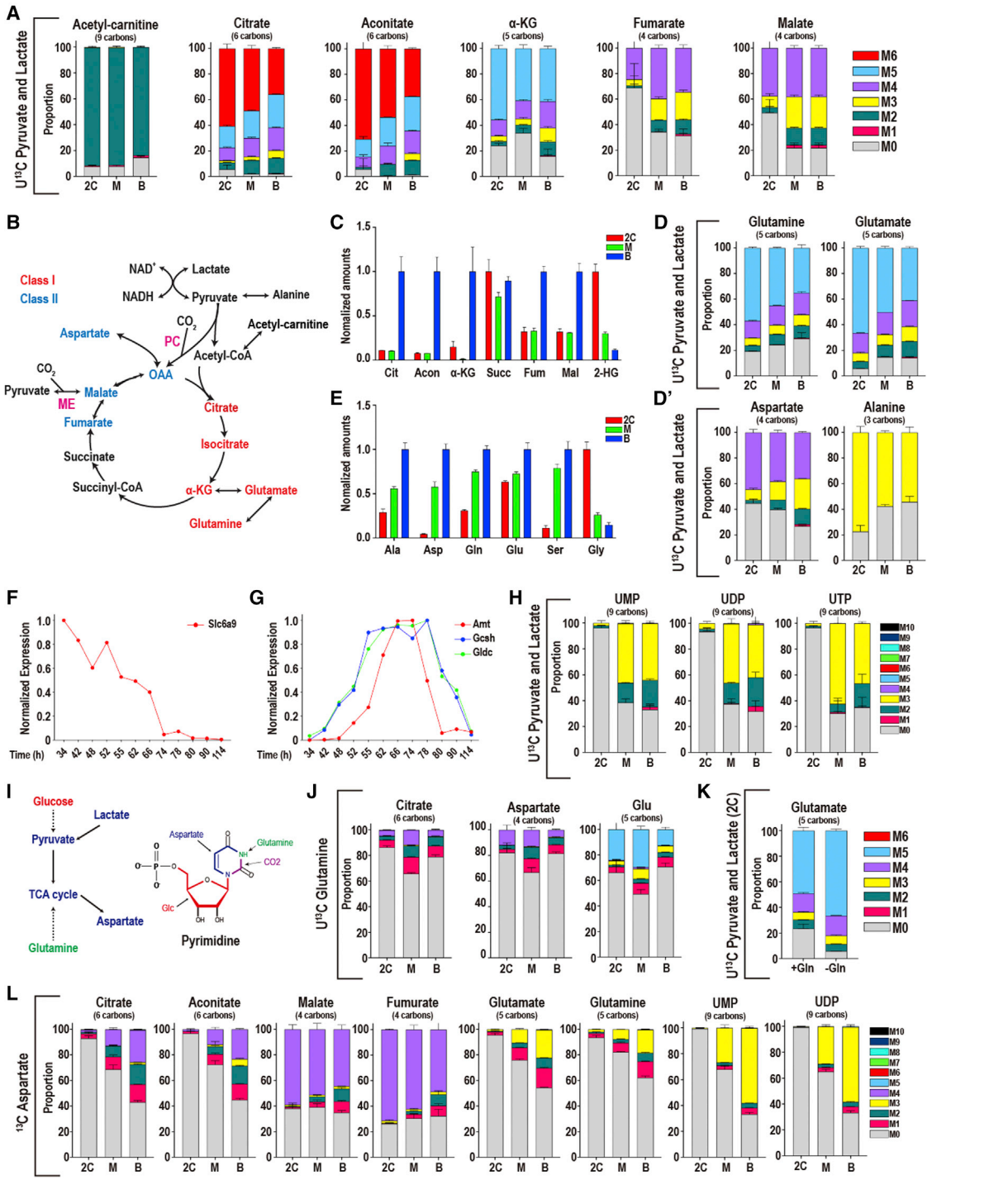

Figure 2. Pyruvate and lactate metabolism during preimplantation development

(A) Isotopologue contributions of pyruvate and lactate to acetyl-carnitine and the TCA cycle metabolites. For acetyl-carnitine, M2 represents the acetyl group. Citrate and aconitate, but not fumarate and malate, are extensively labeled at all stages. The presence of M3 class II metabolites suggests CO_2 fixation via pyruvate carboxylase (PC) or malic enzyme (ME). In all figure panels, stages are represented as 2C: 2-cell, M, morula; B, blastocyst.

(B) Schematic representing the TCA cycle and related amino acids. Class I metabolites are labeled red, and class II metabolites labeled blue.

(C) Normalized amounts of TCA intermediates at each stage (see Table S1 for non-normalized amounts).

(D and D′) Isotopologue contributions to the amino acids Glu, Gln, Ala, and Asp.

(E) Normalized amounts of non-essential amino acids at each stage (see Table S1 for non-normalized amounts).

(F and G) The glycine transporter Slc6a9 (F) peaks in gene expression earlier than the enzymes of the glycine cleavage system (G).

(H) U-^{13}C pyruvate and U-^{13}C lactate contribute to pyrimidine formation at later stages.

(legend continued on next page)

The most prominent U^{13}C glucose-derived nucleotide isotopologue is M5 (accounting for the 5 labeled carbons of the ribose sugar), but not higher than M5, indicating that the nucleobases are not labeled by glucose (Figures 1K and S1I; see Figure S1H for scheme). Consistent with this conclusion, the glycine pool, required for *de novo* purine nucleobase synthesis, does not derive labeled carbons from glucose (Figure S1G). Thus, an endogenous source, such as maternal glycine or salvage of bases, is utilized for nucleobase formation. This is confirmed by labeling experiments in which U^{13}C glycine is provided to the embryo at the zygote stage in the presence or absence of (unlabeled) glucose and then metabolites are harvested at the morula stage. In the presence of glucose, U^{13}C glycine contributes to the generation of M2-M4 isotopologues of purine nucleotides. However, in media in which glucose is absent, no labeled purine nucleotide isotopologue was detected. The base part of the purine requires the synthesis of the ribose sugar first. With glucose absent, the ribose is not made, and thus, glycine, although present in its labeled form, is unable to contribute to the purine base either (Figure 1L). In conclusion, purine nucleobases are derived in part from endogenous glycine, whereas ribose sugars are derived from exogenously provided glucose.

When embryos were provided with [1, 2] ^{13}C glucose, in place of U^{13}C glucose, both M1 and M2 nucleotides were evident, suggesting a complex pattern of ribose-5-phosphate formation, with both the oxidative PPP and non-oxidative PPP providing carbon for nucleotide formation (Figures 1N and 1M for scheme). When embryos were only provided with [1, 2] ^{13}C glucose for 26 h prior to the blastocyst stage, nucleotide synthesis from glucose was greater at the blastocyst stage than at the 2C stage (Figure 1N), yet, it was less than when the label was present for 76 h, suggesting that the nucleotide, or glycogen, pool turns over slowly.

A majority of the purine and pyrimidine biosynthetic genes increase in expression as development proceeds. Genes such as *Gart*, *Paics*, *Impdh*, *Pfas*, and *Atic* participate in multiple steps in purine biosynthesis (Lane and Fan, 2015), and they peak in expression at the morula and early blastocyst stages (Figures S1K and S1L). Pyrimidine synthesis genes, such as *Cad* and *Umps* that function in important steps in the *de novo* pathway, peak at the 4–8 cell stages (Figure 1O). Genes involved in the purine nucleotide cycle, *Adss*, *Adsl*, and *Ampd3*, show an opposite trend in that their expression peaks during the early stages and either declines (for *Adss* and *Ampd3*) or plateaus (for *Adsl*) later in development (Figures S1L and S1M). These genes help maintain a balanced adenine nucleotide pool and as byproducts of this cycle, they also generate fumarate and ammonia (Aragón et al., 1981) (Figure S1N for scheme).

Genes for purine degradation enzymes (*Xdh*, *Ada*, *Gda*, *Pnp*, *Pnp2*, and *Adk*) are more highly expressed early and decrease in expression as development proceeds (Figure 1P). Whereas genes encoding purine salvage enzymes, such as *Hprt* and *Aprt*, show an opposite trend, peaking at the late morula and early blastocyst stages (Figure S1O). Interestingly, hypoxanthine, which is formed by degradation of adenine, and is used by *Hprt* in the salvage pathway of nucleotide synthesis, is barely detectable in 2C embryos, and increases by nearly 100-fold in blastocysts (Figure S1P). These data imply that the capacity of the salvage pathway of purine nucleotide synthesis increases during the course of preimplantation development. In summary, nucleotide synthesis is predominantly a late preimplantation phenomenon, and therefore, the biosynthetic genes appear later in development. The genes encoding degradation enzymes on the other hand are more abundant at the earlier stages. The gene expression data are consistent with earlier biochemical studies on the activities of enzymes that function in purine synthesis, salvage, and degradation (Alexiou and Leese, 1992, 1994).

Pyruvate and lactate metabolism during preimplantation development

We then evaluated the possible contribution of pyruvate/lactate to the TCA cycle. When U^{13}C pyruvate and U^{13}C lactate are provided in the medium, more than 90% (at 2C) and 83% (for blastocysts) of acetyl-carnitine (a surrogate for acetyl-CoA) is the M2 isotopologue (Figures 2A and 2B for scheme). M6 labeled citrate is 61% at the 2C stage with M0 at 6% of the pool (Figure 2A). The proportion of fully labeled citrate decreases from 61% in 2C embryos to 36% in blastocysts. The decrease in M6 citrate is not caused by an increase in M0, which remains almost undetectable, but is associated with a rise in intermediate isotopologues. Aconitate and α-KG show broadly similar labeling patterns as citrate (Figure 2A).

The labeling pattern of malate and fumarate is markedly different from citrate and aconitate (Figure 2A). For example, at the 2C stage, only 37% of malate is fully labeled (M4), and 50% is M0. The amount of malate that is M0 decreases to 22% in blastocysts compared with 50% in 2C embryos. Intermediate isotopologues, such as M3, rise, and account for the changes (M3 is 9% in 2C, 25% in blastocysts). Fumarate shows similar labeling patterns as malate (Figure 2A).

These data show that at all stages pyruvate and lactate are the major players that populate acetyl-CoA, citrate, aconitate, and α-KG, intermediates that are all generated from the "right" half of the cycle (Figure 2B for scheme). However, malate and fumarate, which are formed from the "left" half of the cycle, have a prominent component that remains unlabeled by any exogenous source, particularly during the early stages. The origin of the unlabeled class II metabolites is not currently known, but it is unlikely to be the urea cycle components, which are not expressed in the embryo. The purine nucleotide cycle components, which generate fumarate from aspartate, are highly expressed and constitute a plausible source for the unlabeled class II metabolite pool (Figures S1L and S1M).

The right arm of the TCA cycle includes the "class I" enzymes and metabolites, whereas those associated with the left arm, we

(I) Schematic illustrating the role that glucose, pyruvate, lactate, and glutamine play in forming aspartate and pyrimidine nucleotides.
(J) U-^{13}C Gln only contributes minor amounts of carbon to the TCA cycle and glutamate.
(K) U-^{13}C pyruvate and U-^{13}C lactate generate a majority of Glu in 2C embryos both when exogenous unlabeled Gln (1 mM) is present (+Gln) or absent (−Gln).
(L) In 2C embryos, U-^{13}C Asp contributes to class II metabolites, but not to class I metabolites. In blastocysts, the Asp contribution to class I metabolites increases. U-^{13}C Asp is provided from the zygote stage and is present continuously until metabolites are extracted (see Figure S2J for "pulsed" labeling).
See also Figure S2.

called class II enzymes and metabolites (Nagaraj et al., 2017) (Figure 2B). Class I metabolites contribute to ZGA and are dynamic and highly nutrition sensitive. Class II metabolites are less dynamic and are resistant to nutrient withdrawal. The labeling data show that the disequilibrium, though highest at 2C, and lowest in the blastocyst, is not fully resolved during preimplantation development. This implies a separation of at least a fraction of class I and class II metabolites in different compartments. If oxaloacetate, generated as a class II metabolite, were to be unlabeled, its condensation with fully labeled acetyl-CoA would lead to M2 and not M6 citrate. Since we observe that a large proportion of the citrate generated is M6, we conclude that the unlabeled oxaloacetate needs to be away from the site of citrate synthesis in a different metabolic compartment. As development proceeds, the disequilibrium between class I and class II metabolites lessens, presumably due to increased mixing between the different metabolic pools (Figures 2A and 2C). As we later show, resolution of this disequilibrium coincides with greater metabolic flexibility during development.

No amino acids were included in our culture medium. This allowed us to determine whether pyruvate and lactate present in the media are able to contribute to the formation of amino acids within the embryo. At 2C, only four amino acids (Ala, Asp, Gln, and Glu) are labeled by pyruvate and lactate (Figures 2D, 2D′, and S2A). Among these, Glu and Asp are derived from direct products of the two different arms of the TCA cycle. Glu (derived from α-KG) is only 5% unlabeled, while as much as 45% of Asp (derived from the class II metabolite oxaloacetate) is unlabeled (Figures 2D and 2D′). Several amino acids that are not labeled by pyruvate/lactate, such as Tyr, Phe, and Trp increase dramatically between 2C and blastocyst (Figure S2B). These essential amino acids can rise only if they are derived from increased degradation of endogenous proteins as development proceeds. In contrast, glycine is highest in 2C embryos and decreases substantially in blastocysts (Figure 2E, see also Baltz, 2001), partly due to the high expression of the glycine transporter, *Slc6a9*, prior to our embryo isolation (Figure 2F; Steeves et al., 2003). Following ZGA, the expression of the three enzymes of the glycine cleavage system increases (Figure 2G), which correlates with a fall in glycine levels.

We next determined the role of pyruvate and lactate in nucleotide formation. For both purines and pyrimidines, the ribose moiety is generated from glucose (Figures 1K, S1H, and S1I). The construction of the nucleobases is more complex. Pyruvate and lactate do not contribute carbon to purine nucleobases at any stage (Figure S2C). For pyrimidines, this holds true at the 2C stage. However, later, at the morula stage, there is increased labeling, suggestive of new nucleotide synthesis (Figures 2H and 2I for scheme). Thus, until 2C, the embryos rely on maternally deposited nucleotides, and following ZGA, expression of new enzymes that assist *de novo* nucleotide synthesis gains prominence. Exogenously provided glucose now generates the ribose moiety, while pyruvate-derived and endogenous metabolites combine to generate nucleobases. Together, they form newly synthesized nucleotides.

Gln and Asp, which are critical for multiple biosynthetic reactions, are both formed from pyruvate (Figures 2D and 2D′), although its contribution to Gln is greater than it is to Asp. Following uptake into the cell, Gln is converted to glutamate by the enzyme glutaminase. Both glutaminase isoforms (*Gls* and *Gls2*) are expressed in the embryo, peaking in expression at the 4–8C stage (Figure S2D). To determine a possible contribution of Gln to central carbon metabolites during development, we cultured embryos in normal medium supplemented with 1-mM $U^{13}C$ Gln and found that, at each of the developmental stages, the TCA cycle intermediates, Asp and pyrimidines were largely unlabeled by Gln (Figures 2J, S2E, and S2F). Unlike in cancer cells, Gln plays a minor role here perhaps due to its low uptake and lack of a Gln specific transport system (Gardner et al., 1989; Van Winkle, 2001).

Interestingly, Glu, largely derived from glutamine in most systems, continues to be resourced by pyruvate even when Gln is included in the media (Figure 2K). Furthermore, regardless of whether pyruvate is provided, added Gln cannot rescue the block in development seen upon inhibition of GLUL (glutamine synthetase) that converts Glu to Gln and is expressed at peak levels at the 4–8 cell stage (Figures S2D, S2G, and S2H for scheme). Thus, since Glu is formed from pyruvate (via α-KG), Gln in the embryo is indirectly derived from pyruvate by conversion of Glu to Gln using the essential enzyme GLUL.

Similar to Gln, the amino acid Asp also has a number of critical biosynthetic roles within a cell. In labeling experiments in which $U^{13}C$ Asp is added to the medium, we find that pyrimidine nucleotides, TCA cycle metabolites, and Glu and Gln receive Asp carbons in a stage specific manner (Figure 2L). At the 2C stage, added $U^{13}C$ Asp hardly labels pyrimidine nucleotides, whereas in later-stage embryos, it readily does so, such that in blastocysts, about 60% of UMP, for example, is labeled (Figures 2L and S2J).

$U^{13}C$ Asp efficiently labels malate and fumarate (but not citrate, aconitate, Glu, and Gln) in 2C embryos (Figure 2L). The contribution of Asp to citrate, aconitate, Glu, and Gln is significantly higher in blastocysts (Figure 2L). This is true even when labeled Asp is pulsed for 26 h before measurement, rather than being included from isolation as well (Figure S2J). These results further emphasize the disequilibrium between the Asp-malate-fumarate and the citrate-aconitate-αKG arms of the TCA cycle at 2C (Figure 2B) that is attenuated by the blastocyst stage and supports the model of increased metabolic plasticity with developmental progression.

Adaptation to nutrient conditions

Nutrient deprivation experiments that help decipher metabolic requirements of the embryo have been key in understanding preimplantation metabolism (Biggers et al., 1967; Brown and Whittingham, 1991; Lane and Gardner, 2005). Transcriptomic analysis of either the genome, or a set of identified metabolic genes, both produce an inverted U-shaped trajectory between the early 2C stage and the blastocyst, illustrating that metabolic genes are strictly regulated through development. Pyruvate omission from the zygote stage delays the expression of metabolic genes, while deprivation from the late 2C stage (50 h), when the presence of pyruvate is not obligatory, does not substantially affect their trajectory (Figures 3A, 3A′, S3A, and S3A′).

At both the 2C and morula stages, lactate continues to contribute a majority of carbons to the TCA cycle when pyruvate is withheld (unlabeled citrate: M0 = 14% in 2C, M0 = 4% in morula) (Figures 3B–3C′, S3B, S3D, and S3D′), whereas, the contribution

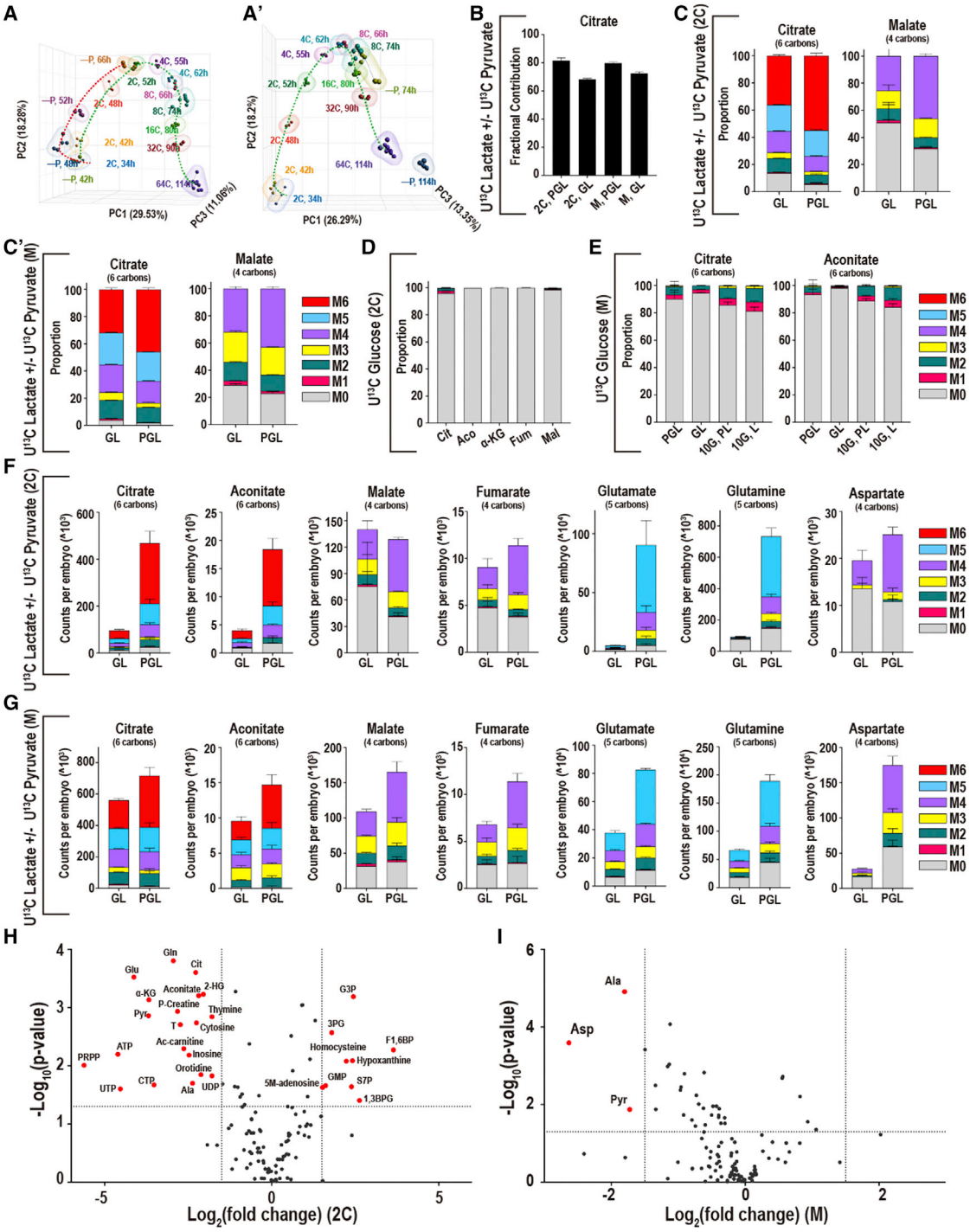

Figure 3. Adaptation to nutrient conditions

(A and A′) Principal-component analysis (PCA) of genes that are directly involved in metabolic processes (1,947 genes) in embryos developing with and without pyruvate. Pyruvate is removed from the zygote stage (A) or the late 2C stage (A′).

(B) In both 2C embryos and morulae, U-13C pyruvate/lactate contributes a majority of carbons to the total citrate pool in the presence (PGL) or absence (GL) of pyruvate.

(C and C′) At both the 2C (C) and morula (C′) stages, the isotopologues of citrate that are formed from U-^{13}C lactate alone (no pyruvate is present, GL) are similar to the isotopologues that are formed when both U-13C pyruvate and U-^{13}C lactate (PGL) are present.

(D and E) The contribution of U-^{13}C glucose to the TCA cycle metabolites remains very low in 2C embryos (D) as well as in morulae (E) in GL media (lacking pyruvate), even when a high amount of glucose (10 mM instead of the normal 0.2 mM) is provided (10G, L).

(legend continued on next page)

of glucose remains very low (unlabeled citrate: M0 = 95% in 2C, M0 = 96% in morula), even when glucose is increased by 50-fold over normal medium levels (Figures 3D, 3E, S3C, and S3E). Thus, pyruvate withdrawal does not cause a switch to glucose-based bioenergetics, instead the TCA cycle continues to be driven by pyruvate that is intracellularly derived from imported lactate (Figures S3F and S3G for scheme).

Pyruvate withdrawal also highlights the disequilibrium between the two halves of the TCA cycle in 2C, but less so, later in development. Upon pyruvate withdrawal, total citrate decreases by 4.8-fold (in 2C) but only 1.3-fold (in morulae), and the fully labeled M6 citrate falls by 7.4-fold (in 2C) but also only 1.8-fold (in morulae). Aconitate also follows a similar pattern (Figures 3F and 3G). In contrast, class II metabolites behave quite differently; malate and fumarate do not decrease significantly in 2C upon pyruvate withdrawal, whereas a small but significant reduction is evident in morulae (Figures 3F and 3G). Metabolites that are associated with energy status, such as phospho-creatine, ATP, and acetyl-carnitine, also decrease in 2C embryos but are unaltered in morulae (Figures 3H and 3I).

The most striking decrease without pyruvate, in 2C embryos, is for the amino acids Gln (8-fold decrease) and Glu (17-fold decrease), whereas for morulae this decrease is less dramatic, Gln (2.8-fold) and Glu (2-fold) (Figures 3F and 3G). Thus, while the synthesis of Glu and Gln is sensitive to pyruvate levels at both stages, 2C embryos are far more sensitive than morulae. Altogether, the above results show that 2C embryos suffer severely from nutrient depletion when pyruvate is withdrawn, whereas morulae are more resistant (Figures 3H and 3I).

Mechanisms of metabolic plasticity

Asp is the only metabolite that decreases upon pyruvate withdrawal in morulae (6-fold), while being stably maintained in 2C embryos (only a 1.2-fold decrease) (Figures 3F and 3G). This dramatic fall in Asp levels in morulae is particularly interesting, given that Asp increases dramatically as development proceeds in the presence of pyruvate, with the levels of Asp 20-fold greater in blastocysts than in 2C embryos (Figure 2E). A number of studies have shown that Asp is highly sensitive to the redox state of the cell (Birsoy et al., 2015; Sullivan et al., 2015), and Asp has an important role in the malate-aspartate (Mal-Asp) shuttle, which impacts the NADH/NAD$^+$ ratio (Lane and Gardner, 2005) (Figure 4A). Thus, the large variance in Asp levels during normal development may signal changes in NADH/NAD$^+$ control mechanisms. A related shuttle, called the glycerol-3P shuttle, is able to fulfill a role similar to the Mal-Asp shuttle (Figure 4B). We find that under normal culture conditions, glycerol-3P, which functions in the glycerol-3P shuttle, falls between the 2C and blastocyst stages (Figure 4C). Flux and directionality of reactions cannot be predicted in this analysis, but the wide range of Asp and glycerol-3P levels at different steps suggests that highly dynamic factors control their levels.

Pyruvate and lactate are interconverted by lactate dehydrogenase that couples their levels to NADH and NAD$^+$ (Williamson et al., 1967). Pyruvate deprivation causes a rise in cytoplasmic NADH, whereas lactate withdrawal raises NAD$^+$ (Veech et al., 2019). In morulae cultured in a pyruvate-free medium (with normal lactate and glucose), Asp levels are 13-fold lower, and glycerol-3P 10-fold higher compared with when only lactate is depleted. Thus, Asp and glycerol-3P are also coupled to NADH/NAD$^+$ (Figures 4D and 4D′). Addition of Gln to the medium does not affect this coupling for glycerol-3P and only partially affects Asp (Figure S4A).

Interestingly, inhibition of the Mal/Asp shuttle enzyme GOT by AOA (aminooxyacetic acid) has no phenotypic consequence for the growth of the embryo if pyruvate is present (Figure 4E), whereas treatment of pyruvate-deprived embryos with AOA blocks development at the morula stage (Figure 4E; see also Lane and Gardner [2005]). Moreover, in previous work, we showed that inhibition of glycolysis (e.g., by inhibiting PFK) blocks development when embryos are deprived of pyruvate, but not when pyruvate is included in the medium (Chi et al., 2020). The block in development of pyruvate deprived and glycolysis inhibited embryos is rescued if the embryos are provided with an alternative means of generating NAD$^+$, and supplementation of the medium with either Asp, which generates NAD$^+$ via the cytoplasmic arm of the Mal-Asp shuttle, or with α-KB, which generates cytoplasmic NAD$^+$ at the level of LDH rescues development (see later, Figure 4F). Furthermore, embryos deprived of glucose have reduced Asp levels, suggesting that lack of NAD$^+$ generation by glucose metabolism can increase the need for Asp-driven NAD$^+$ formation (Figure S4B). Thus, under stress conditions, glucose metabolism, the Mal-Asp shuttle, and pyruvate are all able to generate NAD$^+$ by multiple mechanisms.

Gene expression analysis shows that the enzymes that function in the Mal-Asp and glycerol-3P shuttles display a dynamic expression profile during normal development. For example, *Gpd1l* and *Gpd2* (cytoplasmic and mitochondrial enzymes of the glycerol-3P shuttle, respectively) increase by more than 50-fold between the 2C and morula stages (Figure 4G). Similarly, for the Mal-Asp shuttle, *Mdh1*(cytoplasmic) and *Mdh2* (mitochondrial) increase by approximately 20-fold and 4-fold, respectively, and *Got1* (cytoplasmic) and *Got2* (mitochondrial) enzymes increase by 9-fold and 2.5-fold, respectively, between 2C and blastocyst stages (Figures S4C–S4E).

In contrast to the elevated expression of the shuttle components at later stages, at 2C, by far the most important dehydrogenase that is expected to control the redox balance of the embryo is LDHB, which interconverts lactate/pyruvate and NAD$^+$/NADH (Veech et al., 2019). LDHB activity in the early embryo is 10-fold greater than in any somatic tissue, and its measured activity far exceeds that of all other metabolic enzymes (Brinster, 1965; Epstein et al., 1969). As development proceeds, we detect a striking 2,000-fold decrease in the LDHB mRNA level (Figure 1H). We surmise that the changes in relative levels of the dehydrogenases that control NADH:NAD$^+$ balance

(F and G) Formation of class I metabolites from U-^{13}C lactate/pyruvate decreases when pyruvate is withheld from 2C embryos (F), but less so in morulae (G). Fumarate and malate are less sensitive, and Asp only decreases significantly in morulae.
(H) In 2C embryos 20 metabolites decrease significantly, and 9 metabolites increase upon pyruvate withdrawal (GL).
(I) In morulae, only Asp, pyruvate, and Ala decrease significantly. Metabolites are highlighted if $p < 0.05$ and the log2 fold-change > ±1.5.
See also Figure S3.

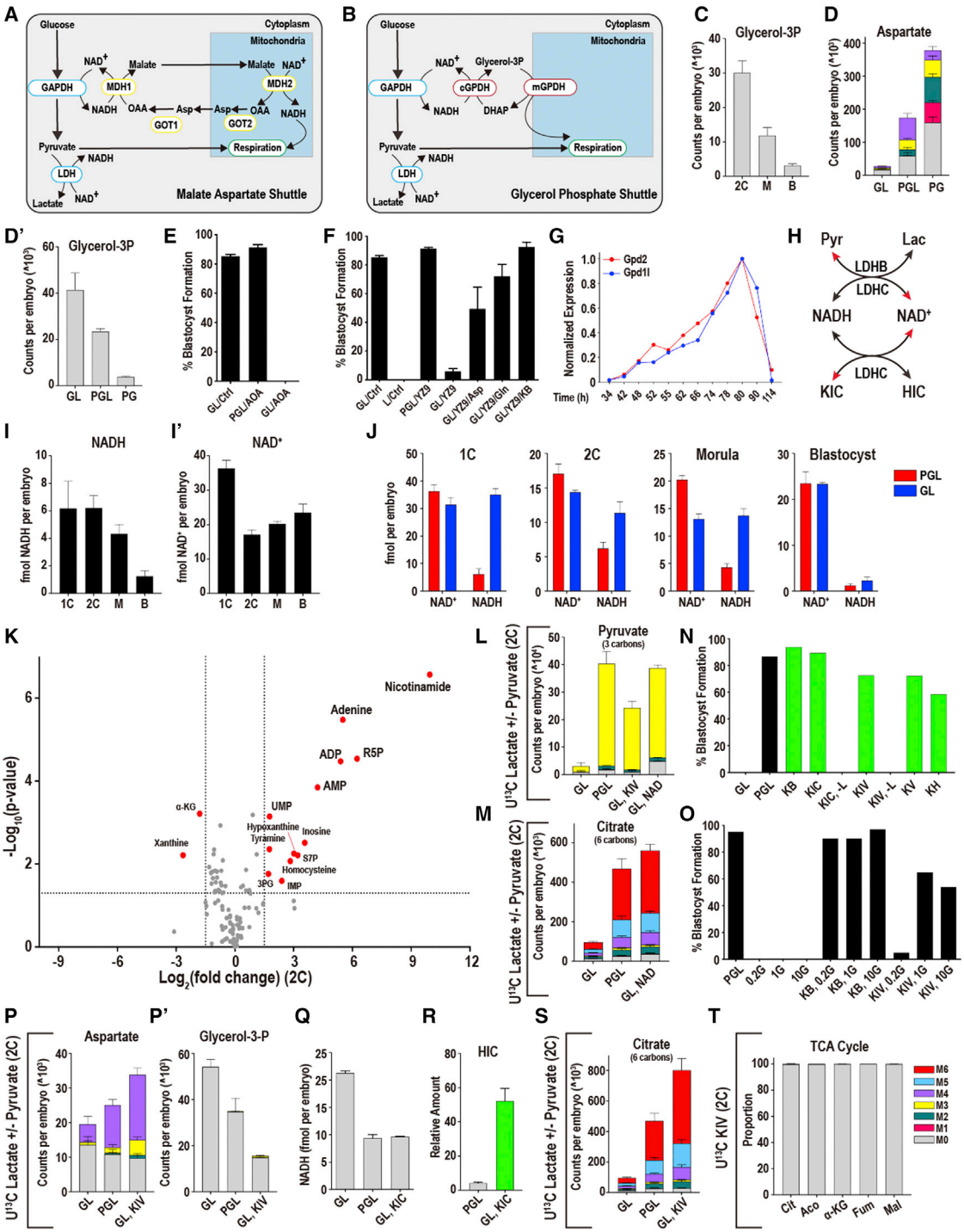

Figure 4. Mechanisms of metabolic plasticity

(A and B) Schematic of the Mal-Asp (A) and glycerol-3P shuttles (B).

(C) The amount of glycerol-3P decreases between the 2C and blastocyst stages.

(D and D′) At the morula stage, Asp increases when lactate is absent (PG) and decreases when pyruvate is withheld (GL). (D′) Glycerol-3P decreases when lactate is absent and increases when pyruvate is withheld.

(E) Following the 2C stage, inhibition of the Mal-Asp shuttle using 0.5-mM AOA does not impact the development of embryos cultured with pyruvate, lactate, and glucose (PGL) but blocks development of embryos cultured in GL media.

(F) The glycolysis inhibitor YZ-9 (2 μM) blocks development of embryos deprived of pyruvate (GL) from the late 2C stage. This block is reversed by the addition of either Asp (1 mM), Gln (1 mM), or α-KB (1 mM).

(G) The glycerol-3P shuttle components Gpd1l and Gpd2 that are expressed in the embryo peak at the morula stage.

(legend continued on next page)

is an important determinant of how NADH:NAD$^+$ impacts, and is impacted by, broader cell metabolism during development. This will affect the flow of carbons between major metabolic pathways. It is reasonable to propose that this change in redox control during normal development is at the core of the increase in metabolic plasticity, defined as flexibility in energetic substrate choice (Folmes et al., 2012), that arises as the embryo advances through the preimplantation process.

NAD$^+$ and NADH in the preimplantation embryo

The above proposal is testable by direct measurement of NAD$^+$ and NADH at different developmental stages (Figures 4I and 4I′). We find, in agreement with similar studies (Kuwahara and Chaykin, 1973), that NAD$^+$ falls markedly between 1C (26 h) and 2C (48 h) and then gradually rises through the blastocyst. In contrast, the fall of NADH between 1C and 2C is rather minor, but its level continues to drop through the blastocyst. Consequently, the total levels of NADH and NAD$^+$ (designated NAD(H)) drop dramatically between 1C and 2C and remain relatively constant thereafter (Figures 4I and 4I′). As development proceeds, the total NAD(H) pool becomes more oxidized.

As described above, under normal growth conditions, NAD$^+$ drops precipitously between 1C and 2C as it is removed from the system by a hydrolase (Nikiforov et al., 2015). Upon pyruvate withdrawal at isolation (1C), NADH levels increase markedly within 6 h (Figure 4J) (see also Dumollard et al. [2007]), yet NAD$^+$ levels do not fall further with the NADH rise. As a result, the total NAD(H) pool in the 1C embryo increases. We presume this is because a rise in NADH upon pyruvate withdrawal also reduces the substrate level for the hydrolase responsible for NAD$^+$ degradation, and this attenuates the degradation of NAD$^+$ seen at this stage under normal conditions.

In contrast to the 1C stage, in 2C (with pyruvate withdrawn at isolation) or morula (pyruvate removed from late 2C) NAD$^+$ levels do fall as NADH levels rise (Figure 4J). Thus, between 2C and morula, the total NAD(H) pool remains the same size regardless of the cytoplasmic redox state. At the blastocyst stage, unlike for 1C, 2C, and morula-stage embryos, pyruvate withdrawal from the morula stage causes only a minor increase in NADH, and NAD$^+$ dominates total NAD(H) with or without pyruvate (Figure 4J). In absolute terms, the rise of NADH following pyruvate withdrawal is more than 25-fold greater in 1C embryos compared with blastocysts (29 fmol increase in NADH in 1C versus 1 fmol in blastocysts) and demonstrates the wide variability of responses to reductive stress at different stages of development.

It was reported that addition of NAD$^+$ to the medium improves development of pyruvate-deprived 2C embryos (Streffer et al., 1974). In a similar experiment with 1C, we find that a rescue to morula is possible, but only when 20-fold more NAD$^+$ is added than what was reported for 2C. Furthermore, exogenously added NAD$^+$ is not able to support development beyond the morula to the blastocyst stage (Figures S4F–S4H). Provision of NADH, nicotinamide, nicotinic acid, NADPH, or NADP$^+$ do not provide a rescue to the morula as seen for NAD$^+$, indicating that exogenous NAD$^+$ acts by increasing the intracellular NAD$^+$ pool and permitting lactate to pyruvate conversion (Figure S4I). Metabolomics show that many of the metabolites that decrease during pyruvate withdrawal are rescued by NAD$^+$ (Figure 4K). NAD$^+$ provision restores pyruvate levels, and the pyruvate and citrate thus generated receive carbons from the labeled lactate (Figures 4L and 4M). NAD$^+$ breakdown products are also detected (Figure S4J).

Rebalancing redox ratios during early stages of development

The premise that a change in redox control during normal development is responsible for the increase in metabolic plasticity is testable by using various α-ketoacids, some naturally occurring and others not, to mimic the effects of pyruvate as a substrate of

(H) Schematic showing how pyruvate and lactate, and α-KIC and HIC, control NADH and NAD$^+$ levels.
(I and I′) NAD$^+$ and NADH levels in 1C, 2C, morulae (M), and blastocysts (B). (I) NADH levels decrease during development, whereas (I′) NAD$^+$ falls markedly between the 1C and 2C stages then rises between the 2C and blastocyst stages. n = 4 biological replicates with ~100 embryos per replicate.
(J) NAD$^+$ and NADH levels in embryos grown with and without pyruvate at different stages of development.
(K) In 2C embryos, provision of 5-mM NAD$^+$ to pyruvate-deprived embryos (GL, +5-mM NAD$^+$) restores the levels of many metabolites that fall when pyruvate is omitted from the media (compare with Figure 3H). A subset of metabolites increases, including breakdown products of NAD$^+$ (e.g., adenine and nicotinamide). Metabolites are highlighted if $p < 0.05$ and the log2 fold-change > ±1.5.
(L) 5-mM U-^{12}C NAD$^+$ or 1-mM U-^{12}C KIV restores pyruvate levels in 2C embryos deprived of pyruvate by facilitating the use of U-13C lactate.
(M) U-^{12}C 5-mM NAD$^+$ restores citrate levels in 2C embryos deprived of pyruvate by facilitating the use of U-^{13}C lactate. The PGL (U-^{13}C pyruvate and U-^{13}C lactate) and GL (U-^{13}C lactate) control samples are shared with Figure 3F because these experiments were performed at the same time.
(N) Alternative α-ketoacids (1 mM) allow zygotes to develop into blastocysts in the absence of pyruvate, as long as lactate is provided. In a medium lacking pyruvate (GL), embryos do not form blastocysts unlike embryos that are cultured with pyruvate (PGL). The conditions represented by green bars all lack pyruvate (−P). The α-ketoacids KB, KIC, KIV, KV, and KH all rescue (−P) embryos unless both pyruvate and lactate are absent (KIC, −L) (KIV, −L). Glucose (G) is present in all samples above, and pyruvate is absent in all samples except control (PGL).
(O) Embryos that are transferred into pyruvate and lactate free media at the late 2C stage (after ZGA) (50 h) are not viable over a range of glucose concentrations (0.2 mM [0.2G], 1 mM [1G], or 10 mM [10G]) unless an α-ketoacid, such as KB or KIV, is provided.
(P and P′) In 2C embryos, aspartate decreases and glycerol-3P increases in GL (U-^{13}C lactate, U-^{12}C glucose) media. KIV fully restores Asp levels and decreases the amount of glycerol-3P. The PGL (U-^{13}C pyruvate and U-^{13}C lactate), and GL (U-^{13}C lactate) controls are shared with Figure 3F as these experiments were performed at the same time.
(Q) NADH levels in zygotes with pyruvate, lactate, and glucose (PGL), glucose and lactate (GL), or (R) Hydroxycaproate (HIC) increases in embryos that are provided with KIC.
(S) U-^{12}C KIV restores citrate levels in 2C embryos deprived of pyruvate by facilitating the use of U-^{13}C lactate. The PGL (U-^{13}C pyruvate and U-^{13}C lactate) and GL (U-^{13}C lactate) control samples are shared with Figure 3F because these experiments were performed at the same time.
(T) U-^{13}C KIV does not contribute carbon to the TCA cycle in 2C embryos cultured in GL media.
See also Figure S4.

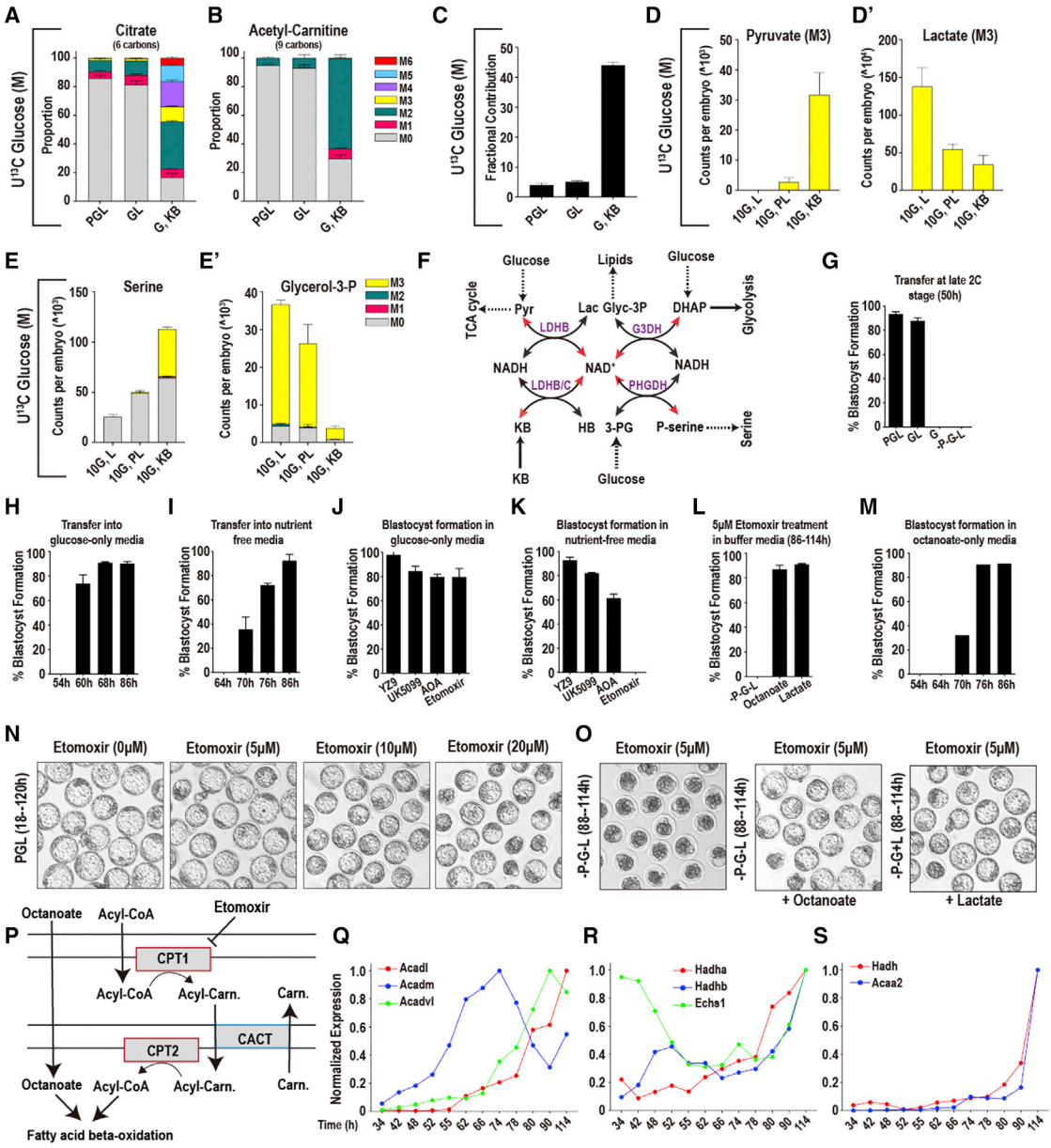

Figure 5. Further metabolic plasticity in later-stage embryos

(A and B) 10-mM U-^{13}C glucose contributes insignificant amounts of carbon to citrate (A) and acetyl-carnitine (B) in morulae in either PGL or GL media. In contrast, glucose contributes substantially with both pyruvate and lactate omitted if α-KB is provided. The control samples are shared with Figure 3E because these experiments were performed at the same time.

(C) For embryos cultured in PGL or GL, 10-mM U-^{13}C glucose contributes a minor amount of carbon to the total citrate pool. However, with both pyruvate and lactate omitted, and α-KB provided, glucose contributes substantially to citrate.

(D–E′) Metabolic reprogramming by α-ketoacid treatment. Pyruvate that is generated from glucose (M3) increases (D) in morula-stage embryos when both pyruvate and lactate are omitted and α-KB is provided from the 2C stage. Lactate generated from glucose (M3) decreases (D′), serine synthesis from glucose increases (E), and glycerol-3P (E′) decreases.

(F) Schematic illustrating how a change in the amount of pyruvate, lactate, or α-KB that is provided to the embryo impacts NAD^+ and NADH levels, and how this, in turn, impacts the activity of other metabolic pathways.

(G) At the late 2C stage (50 h) pyruvate-deprived embryos require both glucose and lactate to form blastocysts.

(H) Glucose alone, without pyruvate and lactate, can support blastocyst formation after the mid-4C stage (60 h).

(I) After 70 h (compacting morulae) embryos form blastocysts in the absence of all three nutrients (-P-G-L).

(J) Embryos transferred from PGL into glucose-only media at 86 h are insensitive to inhibition of glycolysis (YZ9, 2 μM), pyruvate entry into the mitochondria (UK5099, 1 μM), the Mal-Asp shuttle (AOA, 0.5 mM), and FAO (etomoxir, 5 μM).

(K) In the absence of all nutrients the embryos remain insensitive to inhibition of glycolysis, pyruvate transport, and the Mal-Asp shuttle but are highly sensitive to FAO inhibition (etomoxir) and are unable to form blastocysts.

(legend continued on next page)

LDH. Pyruvate (α-ketopropionate) is the simplest of all α-ketoacids that have a direct linkage between a ketone and a carboxyl functional group. A number of studies have shown that a mimic such as α-KB (α-ketobutyrate) is readily taken up by cells and reduced by LDHB (Sullivan et al., 2015). This process generates NAD^+ and α-hydroxybutyrate and provides a way to alter the redox status of the cell. Another isoform of LDH, LDHC, also present in the embryo (Figure 1H; Coonrod et al. [2006]), is highly promiscuous and is able to use α-KB, but also a wider range of α-ketoacids, such as α-KIV (α-ketoisovalerate) and α-KIC (α-ketoisocaproate), which are not substrates for LDHB. Even α-ketoacids, such as α-KV (α-ketovaleric acid), that have no known function in mammalian cells are effective substrates for LDHC. In biochemical assays such α-ketoacids are reduced by LDHC, as they generate NAD^+ and their corresponding α-hydroxyacids (Blanco et al., 1976). Thus, in principle, the presence of LDHC affords us the capability to modulate NAD^+ and NADH independently of the lactate/pyruvate interconversion that is dominated by LDHB. When pyruvate deprived zygotes (1C) are provided with a range of α-ketoacids, α-KB, α-KIV, α-KIC, α-KV, or α-KH, they no longer block at the 2C stage and are able to make blastocysts (Figure 4N). α-ketoacids cannot rescue development of 1C embryos if both pyruvate and lactate are absent (Figure 4N). The rescue by multiple α-ketoacids that are known substrates of LDHC lends credibility to the idea that rebalancing redox is an important mechanism underlying developmental progression.

Unlike 1C, late-2C embryos provided with glucose and an α-ketoacid develop at normal rates to blastocysts even when lactate and pyruvate are both absent. However, embryos that are provided with only glucose but no α-ketoacid die rapidly (Figure 4O). α-KIV is also able to restore development but requires higher amounts of glucose. Multiple lines of evidence establish that α-ketoacids provided to preimplantation embryos allow them to generate NAD^+ and consume NADH. First, when embryos are provided with, for instance, α-KIV, the changes in Asp and glycerol-3P levels that are caused by pyruvate withdrawal are fully rescued (Figures 4P and 4P′). Second, providing α-ketoacids to the embryo prevents the increase in total NADH that is observed when pyruvate is withheld (Figure 4Q). For example, the more than 2-fold increase in NADH levels caused by pyruvate withdrawal in 2C embryos is reverted upon addition of α-KIC to the normal level that is seen in the presence of pyruvate (Figure 4Q). Finally, when an α-ketoacid is included in the medium, a high level of the corresponding α-hydroxyacid is detected. For example, in the presence of α-KIC the level of its α-hydroxyacid, α-HIC, which can only form in a redox related reaction, increases by more than 12-fold (Figure 4R).

The findings in the previous sections are in complete agreement with labeling data that show that when pyruvate-deprived embryos are provided with $U^{13}C$ lactate and unlabeled α-KIV, lactate continues to contribute a majority of carbon to the TCA cycle and its associated amino acids (Figures 4S and S4M–S4O). Indeed, under conditions of pyruvate withdrawal, α-KIV-treated embryos have 14-fold more M6 citrate labeled by lactate compared with embryos not provided with an α-ketoacid (Figure 4S). Importantly, ^{13}C α-KIV does not label the TCA cycle and is therefore not used as a nutrient, but only for the purpose of redox rebalance (Figure 4T). Finally, α-KIV fully rescues the drop in pyruvate, and other metabolites that fall when pyruvate is withdrawn from the media, and isotopologue analysis shows that lactate provides the carbon for the recovered pyruvate (Figures 4L and S4L). Thus, α-KIV acts by facilitating lactate to pyruvate conversion, and the results establish that α-ketoacids rescue development by a redox mediated mechanism. We conclude that at all development stages, lactate can substitute for pyruvate, but only if the cytoplasmic redox state is correctly balanced (Figure S4K).

Normally $U^{13}C$ glucose does not label TCA cycle components and acetyl-CoA (Figure 1I). Strikingly, with pyruvate and lactate both absent but with α-KB provided for redox balance, $U^{13}C$ glucose becomes a significant donor of carbons to the TCA cycle and to acetyl-CoA (Figures 5A–5C and S5A). 83% of the citrate pool is now either fully or partially labeled by carbons from glucose. Similarly, 63% of the acetyl-CoA (judged by M2 acetyl-carnitine) is labeled by glucose (Figure 5B). The rise in labeling of acetyl-CoA coincides with a large increase in the amount of glucose labeled pyruvate and decrease in glucose labeled lactate (Figures 5D and 5D′).

When unlabeled pyruvate and lactate are included in the media they will exchange with labeled pyruvate and lactate that are generated from glucose in the embryo. Glucose-derived pyruvate increases when pyruvate and lactate are removed from the medium partly because of lack of exchange with extracellular unlabeled pyruvate. It is harder to justify how such a lack of exchange might lead to a fall in glucose-derived lactate. The simplest explanation that conforms to the results is that α-ketoacid treatment modulates the intracellular NAD^+/NADH ratio which in turn impacts the pyruvate to lactate ratio. An α-ketoacid-mediated change in intracellular redox state is supported by changes in the activity of other biosynthetic pathways whose activity are linked to the activity of NAD(H) coupled dehydrogenases (Figures 5E, 5E′, and 5F for schematic).

Even with a redox balancer added, glucose is not as efficient as pyruvate/lactate in providing carbons for bioenergetic purposes (Figures 2A, 5A, and 5B). With redox rebalance, glucose-derived carbons mix with carbons from unlabeled sources that enter the TCA cycle pool as acetyl-CoA groups and perhaps at other anaplerotic entry points. In other systems, such as ESCs and cancers, Gln plays this role, but that is not true for the embryo since the contribution of Gln to the TCA cycle remains unchanged under these conditions (Figure S5B).

(L and O) Both octanoate (200 μM) and lactate (2.5 mM) compensate for FAO inhibition (etomoxir, 5 μM).
(M) Pre-8C embryos do not form blastocysts in nutrient-free media supplemented with 200 μM octanoate.
(N) Inhibition of FAO (etomoxir, 5 μM) does not inhibit blastocyst formation in normal PGL media.
(P) Schematic illustrating the transport of octanoate (medium-chain) and long-chain fatty acids (called acyl-CoA in scheme) across the mitochondrial membranes and representing how etomoxir inhibits long-chain acyl-CoA transport, but not the transport of octanoate.
(Q–S) Genes encoding enzymes of mitochondrial β-oxidation show high levels of expression in late morulae and blastocysts.
See also Figure S5.

Further metabolic plasticity in later-stage embryos

Late-2C-(50 h)- or early-4C-(54 h)-stage embryos are non-viable when both pyruvate and lactate are removed from the medium, and embryos do not survive using glucose alone (Figure 5G). However, we find that when transferred to a glucose-only medium at 60 h (mid-4C), 80% of the embryos are able to develop into blastocysts, and when transferred at the uncompacted 8C stage (68 h), all the embryos that are grown without pyruvate and lactate develop into blastocysts (Figures 1A and 5H). Therefore, as development proceeds, the nutrient requirement becomes more flexible such that by the 8C stage, glucose alone is sufficient to sustain development even in the absence of an α-ketoacid. Remarkably, at the 8–16C stage (76 h), 70% of the embryos are able to develop into blastocysts without the provision of any nutrients from the environment (Figure 5I). Following 86 h (late morula, 32C), 100% of the embryos form fully expanded blastocysts (114 h) without any exogenously provided nutrients: pyruvate, lactate, or glucose (Figures 1A and 5I).

To determine how late-stage (86 h) embryos can possibly continue development either in the presence of glucose alone, or more so, how they continue development for up to 2 days beyond that without any exogenously provided nutrients, we used inhibitors of specific metabolic pathways that could potentially point to endogenous moieties that sustain development without any environmental input. Inhibition of the Mal-Asp shuttle using AOA (Figure 4E) or glycolysis using YZ9 (Figure 4F; Chi et al., 2020) can, under certain culture conditions, block development at early stages. In contrast, morulae (86 h) developing in a medium that contains glucose, or one that is deprived of all nutrients, are refractory to both AOA or YZ9 inhibition (Figures 5J and 5K). Thus, neither the Mal-Asp shuttle nor active glycolysis accounts for the embryo's independence from external nutrients after the morula stage (Figures 5J and 5K).

To our surprise, embryos at this stage (86 h), with or without glucose, can develop into blastocysts even when the mitochondrial pyruvate carrier is inhibited by UK5099 (Figures 5J and 5K). The lack of sensitivity of blastocysts to UK5099 contrasts markedly with zygotes (18 h) or 2C embryos (48 h) that are completely blocked by UK5099 even when they are cultured in all three nutrients (Nagaraj et al., 2017).

Finally, we investigated whether fatty acid oxidation (Dunning et al., 2010) is required under the nutrient-limiting conditions described earlier. The carnitine palmitoyl transferase (CPT) inhibitor etomoxir is highly effective in blocking the transfer of fatty acids into the mitochondrion where they can be used for β-oxidation (Figure 5P). Embryos provided with pyruvate, lactate, and glucose are insensitive to etomoxir and develop into blastocysts even when treated from the zygote stage (Figure 5N). Morulae (86 h) developing in glucose alone are also insensitive to inhibition by etomoxir and develop into blastocysts at the same frequency as untreated embryos (Figure 5J). In stark contrast, the embryos (86 h) that are otherwise able to develop into blastocysts in a medium that lacks all nutrients are entirely non-viable when treated with 5-μM etomoxir (Figures 5K and 5O). This implies that in the absence of other nutrients, fatty-acid oxidation (FAO) plays a critical role in development of later-stage embryos. To test this model, we took advantage of the fact that medium-chain fatty acids, such as octanoate, do not require CPT to enter the mitochondrion. We find that added octanoate fully rescues the developmental block that is caused by simultaneous deprivation of all nutrients and treatment with etomoxir (Figures 5L and 5O). Importantly, the octanoate-fueled capacity for the embryo to survive without added nutrients is a result of increased plasticity at later stages of preimplantation development since adding additional octanoate to a 2C/4C embryo, for example, cannot compensate for the lack of pyruvate, lactate, and glucose (Figure 5M). Thus, it appears that the capacity of the embryo to utilize stored or provided lipids increases as development proceeds.

The important role of FAO during post-morula development led us to investigate the expression profile of genes related to mitochondrial β-oxidation in embryos grown in the control medium. The expression of the acyl-CoA dehydrogenase genes (*Acadm*, *Acadl*, and *Acadvl*), which catalyze the first step in mitochondrial β-oxidation, is severalfold higher in late morulae and blastocysts than it is in the early cleavage stages (Figure 5Q). The mitochondrial trifunctional enzyme components (*Hadha* and *Hadhb*) and crotonase (*Echs1*) increase in expression during the later stages of preimplantation development (Figure 5R). The most impressive increases are for short-chain (S)-3-hydroxyacyl-CoA dehydrogenase (*Hadh*) and medium-chain 3-ketoacyl-CoA thiolase (*Acaa2*), which are the final two components of the β-oxidation spiral (Figure 5S). Thus, all components of mitochondrial fatty acid β-oxidation increase substantially during the course of preimplantation development. The increased expression of the FAO enzymes during development reflects the metabolic reprogramming that facilitates the use of a wider range of resources at progressive stages of maturation.

Metabolic response to reductive stress

The gene expression data presented thus far report the profile of preimplantation embryos cultured under normal conditions. To determine if the transcriptome is sensitive to the nutrient content of the extracellular environment, we cultured embryos without pyruvate either from the zygote to the 2C stage (48 h), or from the late 2C (50 h) to the morula stage (78 h). Overall, the expression of genes in mitochondrial FAO, purine, and pyrimidine synthesis, the TCA cycle, glutamine metabolism, or glycine catabolism do not change as a group at either the 2C or morula stage following pyruvate withdrawal (Figures 6A, 6B, and S6A–S6G). Furthermore, genes that encode enzymes that function in shuttles (such as the Mal-Asp and the glycerol-3P shuttle) that coordinate mitochondrial and cytoplasmic metabolism also do not increase when pyruvate is withdrawn. Rare exceptions to this invariance are seen for *Mdh1* (malate dehydrogenase), *Slc25a13* (mitochondrial aspartate and glutamate transporter), and *Slc25a1* (mitochondrial citrate transporter), which increase by 4-fold, 3-fold, and 8-fold, respectively, following pyruvate withdrawal (Figures 6A and S6E).

Glycolytic genes do not change in their relative expression level in 2C embryos that are cultured from the zygote stage without pyruvate. In stark contrast, we find that at the morula stage, pyruvate omission causes a coordinated increase in the expression of genes encoding glycolytic enzymes (Figure 6C). The largest increases are for *Gapdh* (6-fold), *Eno1* (7-fold), *Pkm* (8-fold), and *Ldha* (7-fold). Interestingly, when embryos are provided with α-KB and glucose (but not pyruvate and lactate), which allows progression past 2C, the glycolytic enzymes do

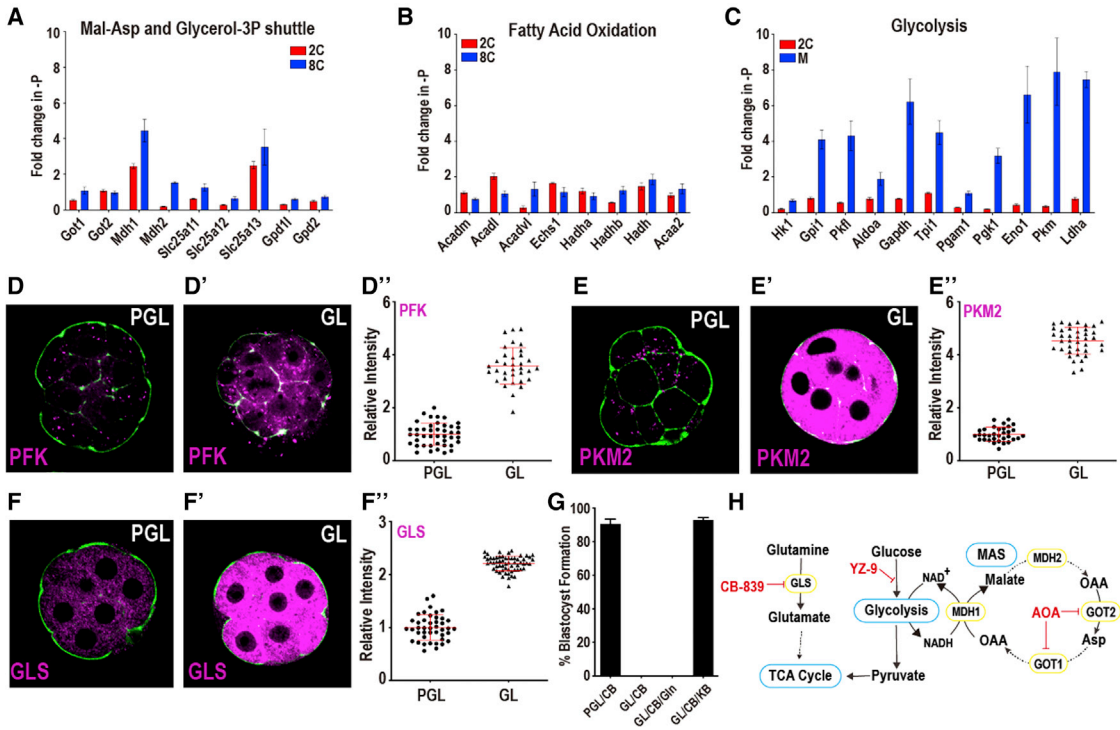

Figure 6. Metabolic response to reductive stress

(A and B) Genes in the Mal-Asp shuttle and glycerol-3P shuttle (A), and mitochondrial beta-oxidation (B) do not show a concerted increase when pyruvate is withdrawn.

(C) The expression level of glycolytic genes increases in morulae, but not in 2C embryos.

(D–E′′) Upon pyruvate withdrawal, protein levels of the glycolytic enzymes PFK (D–D′′) and PKM2 (E–E′′) show significant increases. Data are presented as the mean ± standard deviation (n = ~25 embryos).

(F–F′′) GLS protein increases when pyruvate is withheld. Data are presented as the mean ± standard deviation (n = ~25 embryos).

(G) Glutaminase inhibition (200-nM CB-839) does not block the development of embryos in PGL media. Embryos in GL media, however, block in development following CB-839 treatment. α-KB (1 mM) suppresses the block, but Gln (1 mM) does not.

(H) Schematic representing glycolysis, the Mal-Asp shuttle, glutamine metabolism, and their inhibitors.

See also Figure S6.

not increase in expression in the morula (Figure S6H). To determine whether the increase in RNA levels upon pyruvate withdrawal leads to an increase in protein expression, we stained the embryos using specific antibodies for phosphofructokinase (PFK), glyceraldehyde-3-phosphate dehydrogenase (GAPDH), and pyruvate kinase (PKM2). We find that the protein levels of GAPDH, PFK, and PKM2 increase, with the rise in PKM2 especially marked (Figures 6D–6E′′ and S6I–S6I′′). Thus, following the 2C stage, the embryo responds to pyruvate withdrawal by mounting a coordinated transcriptional response that increases the abundance of glycolytic proteins.

In cultured cancer cells and ESCs, a high level of glycolysis is often coupled with high rates of glutamine consumption. In the embryo, based on the RNA-seq analysis, this seemed unlikely as the transcript levels of *Gls*, *Gls2*, or *Glud1* remain unchanged upon pyruvate withdrawal (Figure S6G). However, a different conclusion arises when the glutaminase (GLS) protein, which converts glutamine to glutamate, is analyzed instead of its invariant RNA. GLS protein levels increase substantially upon pyruvate withdrawal (Figures 6F–6F′′) perhaps by a post-transcriptional mechanism similar to that seen in cancer models (Gao et al., 2009). Inhibition of glutaminase activity with the specific inhibitor CB-839 causes a block in development in pyruvate-deprived embryos but not when pyruvate is present (Figures 6G and 6H for scheme). The block in development caused by the glutaminase inhibitor is rescued when another α-ketoacid is included in the medium in place of pyruvate (Figure 6G). We conclude that the GLS protein level increases in response to reductive stress caused by pyruvate withdrawal, and thereby plays an active role in responding to a high NADH:NAD^+ cellular environment.

Mechanisms of metabolic reprogramming during reductive stress

Next, we investigated and characterized the mechanism by which embryos upregulate glycolysis and glutaminase function in response to pyruvate withdrawal. Studies on other systems find that Myc and HIF-1α play important roles in glycolytic gene expression especially under various stress conditions (Gordan et al., 2007). Immunofluorescence analysis suggests that HIF-1α or HIF-2α are not stabilized in the embryo under any of the conditions that we use in this study (not shown). In contrast, nuclear Myc is detected in abundance in morulae that are deprived of pyruvate (Figures 7A–7A′′). Interestingly, by

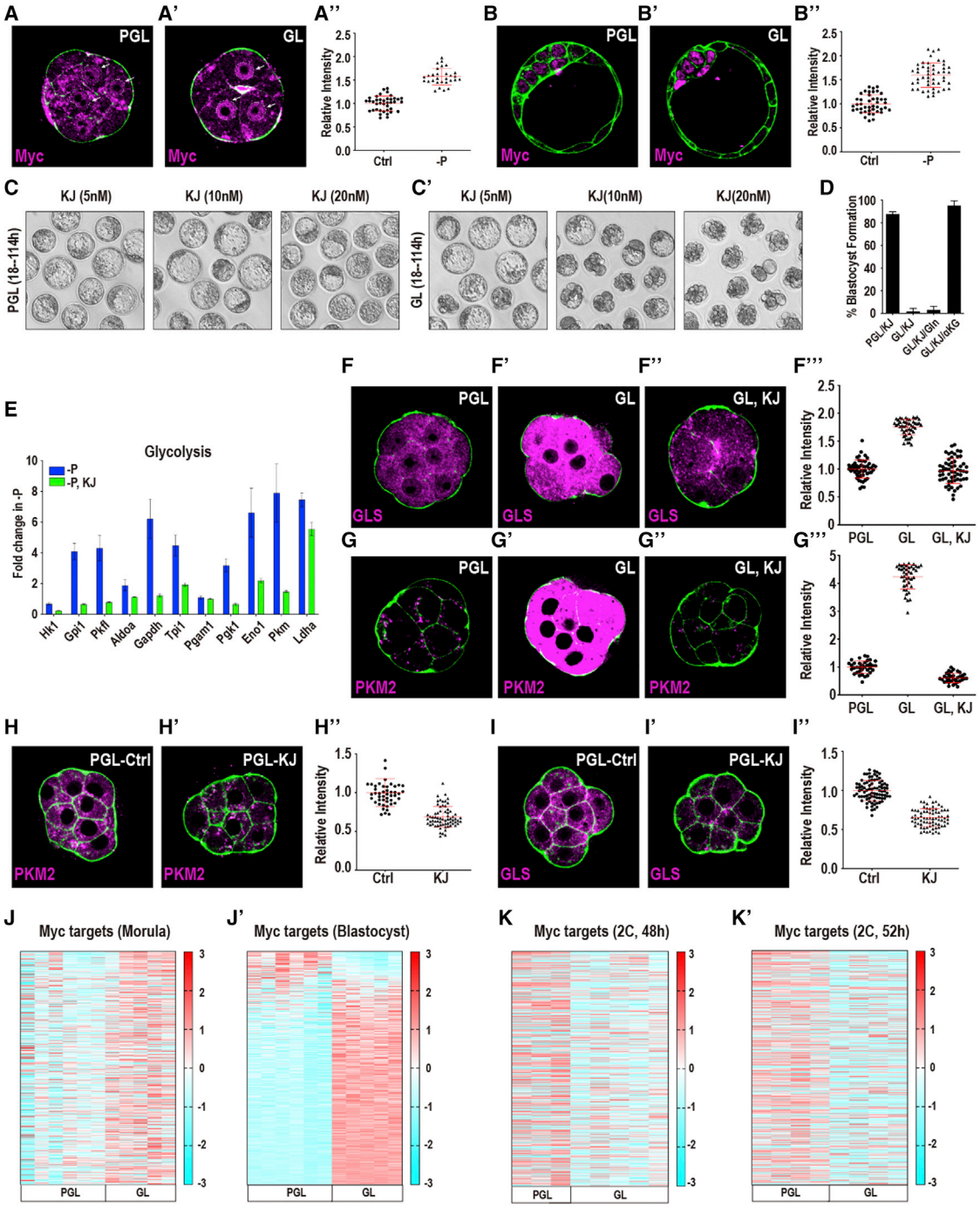

Figure 7. Mechanisms of metabolic reprogramming during reductive stress

(A–B′′) Myc protein localization upon pyruvate withdrawal in the morula and blastocyst. (A–A′′) In morulae, Myc is diffusely expressed in PGL (A) but is nuclearly localized in GL (A′). Quantitation in (A′′). (B–B′′) In blastocysts (114 h), Myc is expressed at low levels in PGL (B). Pyruvate withdrawal causes an increase in Myc expression in the ICM but not in the TE (B′). Quantitation in (B′′). Data are presented as the mean ± standard deviation (n = ~25 embryos).

(C and C′) Embryos cultured from the late 2C stage (50 h) in GL (C′) but not in PGL (C) media block in development when treated with the Myc inhibitor KJ-Pyr-9 (abbreviated as KJ) at varying concentrations.

(D) Embryos cultured in GL are sensitive to KJ (20 nM). Gln (1 mM) does not rescue, but supplementation with (1 mM) α-KG (di-methyl) fully rescues the block.

(E) Glycolytic genes do not increase in expression in pyruvate-deprived embryos that are treated with 20nM KJ (green bars). The inhibitor-free sample (blue) is shared with Figure 6A because these experiments were performed at the same time.

(F–G′′′) Myc inhibition blocks the increase in pyruvate sensitive genes GLS (F–F′′′) and PKM2 (G–G′′′). GLS (F) and PKM2 (G) levels rise in GL media (F′ and G′). KJ (20 nM) prevents this increase in GLS (F′′) and in PKM2 (G′′). Quantitation in (F′′′ and G′′′). Data are presented as the mean ± standard deviation (n = ~25 embryos).

(legend continued on next page)

mechanisms as yet unclear, at the blastocyst stage, Myc expression is limited to the cells of the ICM (Figure 7B; Clavería et al., 2013; Hashimoto and Sasaki, 2019). Pyruvate withdrawal also leads to a robust increase in nuclearly localized ICM specific Myc, while the TE cells remain undetectable for Myc expression (Figures 7B–7B″).

We inhibited the activity of Myc using a specific inhibitor (KJ-Pyr-9, which prevents Myc-Max interaction), in order to assess the functional role of Myc in protecting the embryo during reductive stress. Embryos provided with pyruvate are resistant to treatment with 20-nM KJ-Pyr-9 and readily form blastocysts under these conditions (Figures 7C and 7D). In contrast, without access to pyruvate, embryos are highly sensitive to Myc inhibition and exhibit a complete developmental block prior to the morula stage (Figures 7C′ and 7D). This Myc inhibition also abrogates the increases in glycolytic gene expression and the rise in PKM2 and GLS proteins that is observed following pyruvate withdrawal (Figures 7E–7G‴). There is not a significant block in morula formation when Myc is inhibited under normal culture conditions. However, the protein levels of PKM2 and GLS are significantly reduced upon Myc inhibition even with pyruvate, lactate, and glucose present (Figures 7H–7I″), suggesting a measure of metabolic control by Myc during normal development that becomes far more prominent under conditions of reductive stress.

The above results are substantiated by RNA-seq experiments, which reveal a dramatic upregulation of Myc targets at both the morula and blastocyst stages upon pyruvate withdrawal (Figures 7J and 7J′). We used two independently derived Myc target gene lists: list 1 (Morrish and Hockenbery, 2014) and list 2 (Kim et al., 2008). For either list, 90% of the Myc targets are affected by pyruvate withdrawal (Figure 7J, list 1 and Figure S7B, list 2). Importantly, there is no increase in Myc target genes when embryos are cultured with glucose as the sole nutrient source (with added α-KB) (Figures S7C and S7C′). We also find that Myc target genes do not increase in expression in 2C embryos when pyruvate is withheld from the zygote stage (Figures 7K and 7K′). This result is reasonable since transcription of zygotic genes does not take place under these conditions. This would, in part, explain why early-2C embryos are far more sensitive to pyruvate withdrawal when compared with embryos at later stages of development. Increased expression of Myc targets upon reductive stress is only possible in embryos that have completed ZGA, and before that event, the embryo is unable to respond to stress through the coordinated upregulation of the Myc-related network.

DISCUSSION

Preimplantation mouse embryos have minimal requirements from the environment, and our normal culture medium provides only three nutrients, pyruvate, lactate, and glucose (Nagaraj et al., 2017), and no amino acids, nucleotides, fats, or proteins are included. The 1C/2C stage is rigid and depends on the presence of pyruvate/lactate, whereas later steps show increased metabolic plasticity, and more nutrients can sustain development, to the extent that in the late morula, internally stored fatty acids can sustain the transition to the expanded blastocyst with no externally provided nutrients in the medium.

1C/ 2C embryos provided with lactate alone are unable to convert enough intracellular lactate to pyruvate for it to be used as a nutrient. A large drop in free NAD^+ between 1C and 2C under normal growth conditions contributes to the inability of the pre-ZGA embryo to adapt to reductive stress. Removal of pyruvate from the earliest stage embryos causes a block in development and a concomitant dramatic increase in NADH levels. Thus, a combination of NAD^+ depletion by degradation that is seen during normal development, superimposed upon the additional conversion of NAD^+ to NADH in the absence of pyruvate (reductive stress), leads to very low free NAD^+ that is unable to sustain further development in a pyruvate-free medium.

Beyond 2C, in normal medium, LDHB drops while components of the Mal-Asp shuttle, the glycerol-3P shuttle, and the mitochondrial electron transport chain all increase in abundance, and these assist in the regeneration of NAD^+ that is consumed during lactate to pyruvate conversion. Thus, lactate without added pyruvate can now support development. The inability of added glucose to support pre-8C development on its own, is traced to (among others), low glucose uptake (Leese and Barton, 1984), low glycolytic enzymes/metabolites, and an inefficient transition to lower glycolysis. Only a small amount of pyruvate is generated by the residual glycolysis, which, due to high LDHB, is quickly converted to lactate. NAD^+ is not regenerated at sufficient rates to reconvert lactate to pyruvate before it is exported out. However, a longer-chain α-ketoacid can act as a surrogate to pyruvate, restore NAD^+, disfavor conversion of glucose-derived pyruvate to lactate, and allow the embryo to use glucose as the sole nutrient. Furthermore, redox rebalance also increases the activity of GAPDH, a key glycolytic enzyme, and in turn increase pyruvate generation. Thus, the capacity of the embryo to regulate its redox state controls metabolic plasticity.

The huge excess of LDHB in 1C/2C is of maternal origin and unlike for many other enzymes, the zygotic expression of LDHB and the residual RNA degrades over time. This is compensated by an increase in the shuttle components and the rate of mitochondrial oxygen consumption. Consequently, at the early morula stage, glucose (without added α-ketoacids) is able to support development even when both pyruvate and lactate are absent. Importantly, the ability of embryos to develop without pyruvate and lactate is not due to a switch to a novel glucose-based metabolism but rather represents an increase in plasticity that is facilitated by a decrease in LDHB levels and an increased ability of the embryo to regenerate NAD^+ by alternative means. Metabolic plasticity increases further following compaction as expanded blastocysts can form in the absence of all nutrients,

(H–I″) Myc functions under normal (PGL) growth conditions. Treatment with 20-nM KJ (PGL medium, 2C, 50 h) causes PKM2 (H and H′) and glutaminase (I and I′) protein levels to decrease. Quantitation in (H″ and I″). Data are presented as the mean ± standard deviation (n = ~25 embryos).
(J–K′) A majority of Myc targets increase in expression at the morula stage (J) and more so in blastocysts (J′) following pyruvate withdrawal at the late 2C stage (50 h). (K and K′) Myc targets do not increase in 2C embryos if they are cultured in a medium that lacks pyruvate from the zygote stage.
See also Figure S7.

allowing internal resources to be utilized by FAO as was shown in the pioneering studies of rabbit, cow, and pig embryos, which survive prolonged periods without nutrients (Leese, 2012; Sturmey et al., 2009). In mice, FAO alone cannot support development of cleavage-stage embryos, and a requirement for FAO is not evident when pyruvate, lactate, or glucose are present (consistent with Hillman and Flynn, 1980). Importantly, immediately prior to implantation *in utero*, the late blastocyst moves through a very nutrient poor environment, and FAO is likely to become essential *in vivo* during these very late stages. Finally, several of the metabolic changes upon environmental manipulation are reminiscent of metabolic changes in diapause (Hussein et al., 2020).

Cultured embryos and cancer cells are grown using dissimilar media and this is reflected in their largely distinct nutrient usage. *In vivo* cancer cells may favor lactate as a nutrient (Faubert et al., 2017; Hui et al., 2017), but in general, the metabolisms of the two systems are distinct. It was therefore surprising to find that the Myc-dependent stress response of the embryo is virtually identical to the Myc-dependent gene expression in cancer. It seems that embryos grown under stress situations bring out similarities between developmental and cancer metabolism.

In our previous work on mouse and *Drosophila*, we have found numerous instances of intersections between metabolic and signaling pathways (Chi et al., 2020; Nagaraj et al., 2012; Nagaraj et al., 2017; Owusu-Ansah and Banerjee, 2009). Here, we demonstrate that metabolic enzymes are highly regulated at the transcription level and that changing flexibility and redox state can determine entire developmental programs to the extent that the embryo is able to survive and develop in the absence of pyruvate and lactate if only the redox conditions are altered. The central message is that metabolic processes are not passive bystanders to a developmental program laid down by other cell biological phenomena. Rather, metabolism is a direct and active participant that helps set up developmental programs. In disorders such as early loss of pregnancy, birth defects, diabetes, and aging, it will be important in the future to investigate if defects in metabolic plasticity or redox status, stress-induced or not, is one of the contributing causes.

Limitations of the study

In the future, it will be important to study metabolic plasticity in embryonic development under *in vivo* conditions that reflect the complexity of the oviductal environment. It will also be important to study later developmental consequences of metabolic plasticity. This can be achieved by transferring the embryos cultured under the conditions described here back into pseudo-pregnant recipients to investigate whether metabolic plasticity impacts lineage formation, implantation, and later steps of development. This was beyond the scope of this study but will be the ultimate test of the plasticity model and its purpose under normal and stress related environments during a pregnancy.

STAR★METHODS

Detailed methods are provided in the online version of this paper and include the following:

SUPPLEMENTAL INFORMATION

Supplemental information can be found online at https://doi.org/10.1016/j.devcel.2021.07.020.

ACKNOWLEDGMENTS

We thank Raghavendra Nagaraj, Alice Shapiro, and all members of our laboratory for their suggestions and help. We thank the UCLA Metabolomics Center for their generous help with metabolomics analysis. Sequencing was performed by Suhua Feng of the BSCRC Sequencing Core, and we thank Steve Jacobsen for his support with sequencing. We appreciate many inputs by Tom Graeber, Daniel Braas, Heather Christofk, and Hilary Coller. Christofk and Coller also helped by providing many antibody reagents.

This work was supported by the NIH Director's Pioneer Award to U.B. (DP1DK098059). U.B. is supported by NCI grant R01 CA217608 and NHLBI grant R01 HL067395. F.C. is supported by a China Scholarship Council Award, a California Institute for Regenerative Medicine Predoctoral Fellowship, and the MBI Whitcome Predoctoral Fellowship. M.S.S. was supported by the CTSI Iris Cantor Women's Health Center Award. Finally, we are grateful to Owen Witte and the Broad Stem Cell Research Center for several innovation and research awards to UB and the BSCRC predoctoral fellowship support to F.C. We are particularly grateful to the Gillian S. Fuller Foundation for their support of BSCRC in general and this work in particular.

AUTHOR CONTRIBUTIONS

M.S.S., F.C., and U.B. conceived the project and wrote and discussed the manuscript. M.S.S., F.C., and J.T.H.S. performed experiments. U.B. secured funding and provided mentorship.

DECLARATION OF INTERESTS

The authors declare no competing interests.

Received: October 7, 2020
Revised: April 26, 2021
Accepted: July 28, 2021
Published: August 23, 2021

REFERENCES

Alexiou, M., and Leese, H.J. (1992). Purine utilisation, de novo synthesis and degradation in mouse preimplantation embryos. Development *114*, 185–192.

Alexiou, M., and Leese, H.J. (1994). Enzymes of purine salvage and catabolism in the mouse preimplantation embryo measured by high performance liquid chromatography. J. Reprod. Fertil. *101*, 151–158.

Altman, B.J., Stine, Z.E., and Dang, C.V. (2016). From Krebs to clinic: glutamine metabolism to cancer therapy. Nat. Rev. Cancer *16*, 749.

Aragón, J.J., Tornheim, K., Goodman, M.N., and Lowenstein, J.M. (1981). Replenishment of citric acid cycle intermediates by the purine nucleotide cycle in rat skeletal muscle. Curr. Top. Cell. Regul. *18*, 131–149.

Baltz, J.M. (2001). Osmoregulation and cell volume regulation in the preimplantation embryo. Curr. Top. Dev. Biol. *52*, 55–106.

Barbehenn, E.K., Wales, R.G., and Lowry, O.H. (1974). The explanation for the blockade of glycolysis in early mouse embryos. Proc. Natl. Acad. Sci. USA *71*, 1056–1060.

Biggers, J.D., Whittingham, D.G., and Donahue, R.P. (1967). The pattern of energy metabolism in the mouse oocyte and zygote. Proc. Natl. Acad. Sci. USA *58*, 560–567.

Birsoy, K., Wang, T., Chen, W.W., Freinkman, E., Abu-Remaileh, M., and Sabatini, D.M. (2015). An essential role of the mitochondrial electron transport chain in cell proliferation is to enable aspartate synthesis. Cell *162*, 540–551.

Blanco, A., Burgos, C., Gerez de Burgos, N.M., and Montamat, E.E. (1976). Properties of the testicular lactate dehydrogenase isoenzyme. Biochem. J. *153*, 165–172.

Brinster, R.L. (1963). A method for in vitro cultivation of mouse ova from two-cell to blastocyst. Exp. Cell Res. *32*, 205–208.

Brinster, R.L. (1965). Lactate dehydrogenase activity in the preimplanted mouse embryo. Biochim. Biophys. Acta *110*, 439–441.

Brown, J.J., and Whittingham, D.G. (1991). The roles of pyruvate, lactate and glucose during preimplantation development of embryos from F1 hybrid mice in vitro. Development *112*, 99–105.

Buescher, J.M., Antoniewicz, M.R., Boros, L.G., Burgess, S.C., Brunengraber, H., Clish, C.B., DeBerardinis, R.J., Feron, O., Frezza, C., Ghesquiere, B., et al. (2015). A roadmap for interpreting (13)C metabolite labeling patterns from cells. Curr. Opin. Biotechnol. *34*, 189–201.

Chi, F., Sharpley, M.S., Nagaraj, R., Roy, S.S., and Banerjee, U. (2020). Glycolysis-independent glucose metabolism distinguishes TE from ICM fate during mammalian embryogenesis. Dev. Cell *53*, 9–26.e4.

Clavería, C., Giovinazzo, G., Sierra, R., and Torres, M. (2013). Myc-driven endogenous cell competition in the early mammalian embryo. Nature *500*, 39–44.

Coonrod, S., Vitale, A., Duan, C., Bristol-Gould, S., Herr, J., and Goldberg, E. (2006). Testis-specific lactate dehydrogenase (LDH-C4; Ldh3) in murine oocytes and preimplantation embryos. J. Androl. *27*, 502–509.

Dumollard, R., Ward, Z., Carroll, J., and Duchen, M.R. (2007). Regulation of redox metabolism in the mouse oocyte and embryo. Development *134*, 455–465.

Dunning, K.R., Cashman, K., Russell, D.L., Thompson, J.G., Norman, R.J., and Robker, R.L. (2010). Beta-oxidation is essential for mouse oocyte developmental competence and early embryo development. Biol. Reprod. *83*, 909–918.

Epstein, C.J., Wegienka, E.A., and Smith, C.W. (1969). Biochemical development of preimplantation mouse embryos: in vivo activities of fructose 1,6-diphosphate aldolase, glucose 6-phosphate dehydrogenase, malate dehydrogenase, and lactate dehydrogenase. Biochem. Genet. *3*, 271–281.

Faubert, B., Li, K.Y., Cai, L., Hensley, C.T., Kim, J., Zacharias, L.G., Yang, C., Do, Q.N., Doucette, S., Burguete, D., et al. (2017). Lactate metabolism in human lung tumors. Cell *171*, 358–371.e9.

Folmes, C.D., Dzeja, P.P., Nelson, T.J., and Terzic, A. (2012). Metabolic plasticity in stem cell homeostasis and differentiation. Cell Stem Cell *11*, 596–606.

Gao, P., Tchernyshyov, I., Chang, T.C., Lee, Y.S., Kita, K., Ochi, T., Zeller, K.I., De Marzo, A.M., Van Eyk, J.E., Mendell, J.T., et al. (2009). c-Myc suppression of miR-23a/b enhances mitochondrial glutaminase expression and glutamine metabolism. Nature *458*, 762–765.

Gardner, D.K., Clarke, R.N., Lechene, C.P., and Biggers, J.D. (1989). Development of a noninvasive ultramicrofluorometric method for measuring net uptake of glutamine by single preimplantation mouse embryos. Gamete Res. *24*, 427–438.

Gordan, J.D., Thompson, C.B., and Simon, M.C. (2007). HIF and c-Myc: sibling rivals for control of cancer cell metabolism and proliferation. Cancer Cell *12*, 108–113.

Hashimoto, M., and Sasaki, H. (2019). Epiblast formation by TEAD-YAP-dependent expression of pluripotency factors and competitive elimination of unspecified cells. Dev. Cell *50*, 139–154.e5.

Hillman, N., and Flynn, T.J. (1980). The metabolism of exogenous fatty acids by preimplantation mouse embryos developing in vitro. J. Embryol. Exp. Morphol. *56*, 157–168.

Hui, S., Ghergurovich, J.M., Morscher, R.J., Jang, C., Teng, X., Lu, W., Esparza, L.A., Reya, T., Le Zhan, Z., Yanxiang Guo, J., et al. (2017). Glucose feeds the TCA cycle via circulating lactate. Nature *551*, 115–118.

Hussein, A.M., Wang, Y., Mathieu, J., Margaretha, L., Song, C., Jones, D.C., Cavanaugh, C., Miklas, J.W., Mahen, E., Showalter, M.R., et al. (2020). Metabolic control over mTOR-dependent diapause-like state. Dev. Cell *52*, 236–250.e7.

Intlekofer, A.M., and Finley, L.W.S. (2019). Metabolic signatures of cancer cells and stem cells. Nat. Metab. *1*, 177–188.

Jang, C., Chen, L., and Rabinowitz, J.D. (2018). Metabolomics and isotope tracing. Cell *173*, 822–837.

Kim, J., Lee, J.H., and Iyer, V.R. (2008). Global identification of Myc target genes reveals its direct role in mitochondrial biogenesis and its E-box usage in vivo. PLoS One *3*, e1798.

Kuwahara, M., and Chaykin, S. (1973). Biosynthesis of pyridine nucleotides in early embryos of the mouse (Mus musculus). J. Biol. Chem. *248*, 5095–5099.

Lane, A.N., and Fan, T.W. (2015). Regulation of mammalian nucleotide metabolism and biosynthesis. Nucleic Acids Res. *43*, 2466–2485.

Lane, M., and Gardner, D.K. (2005). Mitochondrial malate-aspartate shuttle regulates mouse embryo nutrient consumption. J. Biol. Chem. *280*, 18361–18367.

Leese, H.J. (2012). Metabolism of the preimplantation embryo: 40 years on. Reproduction *143*, 417–427.

Leese, H.J., and Barton, A.M. (1984). Pyruvate and glucose uptake by mouse ova and preimplantation embryos. J. Reprod. Fertil. *72*, 9–13.

Leung, C.Y., Zhu, M., and Zernicka-Goetz, M. (2016). Polarity in cell-fate acquisition in the early mouse embryo. Curr. Top. Dev. Biol. *120*, 203–234.

Liberti, M.V., and Locasale, J.W. (2016). The Warburg effect: how does it benefit cancer cells? Trends Biochem. Sci. *41*, 211–218.

Martin, K.L., and Leese, H.J. (1995). Role of glucose in mouse preimplantation embryo development. Mol. Reprod. Dev. *40*, 436–443.

Morrish, F., and Hockenbery, D. (2014). MYC and mitochondrial biogenesis. Cold Spring Harb. Perspect. Med. *4*, a014225.

Nagaraj, R., Gururaja-Rao, S., Jones, K.T., Slattery, M., Negre, N., Braas, D., Christofk, H., White, K.P., Mann, R., and Banerjee, U. (2012). Control of mitochondrial structure and function by the Yorkie/YAP oncogenic pathway. Genes Dev. *26*, 2027–2037.

Nagaraj, R., Sharpley, M.S., Chi, F., Braas, D., Zhou, Y., Kim, R., Clark, A.T., and Banerjee, U. (2017). Nuclear localization of mitochondrial TCA cycle enzymes as a critical step in mammalian zygotic genome activation. Cell *168*, 210–223.e11.

Nikiforov, A., Kulikova, V., and Ziegler, M. (2015). The human NAD metabolome: functions, metabolism and compartmentalization. Crit. Rev. Biochem. Mol. Biol. *50*, 284–297.

Owusu-Ansah, E., and Banerjee, U. (2009). Reactive oxygen species prime Drosophila haematopoietic progenitors for differentiation. Nature *461*, 537–541.

Pavlova, N.N., and Thompson, C.B. (2016). The emerging hallmarks of cancer metabolism. Cell Metab. *23*, 27–47.

Picelli, S., Faridani, O.R., Björklund, A.K., Winberg, G., Sagasser, S., and Sandberg, R. (2014). Full-length RNA-seq from single cells using Smart-seq2. Nat. Protoc. *9*, 171–181.

Rossant, J. (2018). Genetic control of early cell lineages in the mammalian embryo. Annu. Rev. Genet. *52*, 185–201.

Steeves, C.L., Hammer, M.A., Walker, G.B., Rae, D., Stewart, N.A., and Baltz, J.M. (2003). The glycine neurotransmitter transporter GLYT1 is an organic

osmolyte transporter regulating cell volume in cleavage-stage embryos. Proc. Natl. Acad. Sci. USA *100*, 13982–13987.

Streffer, C., Elias, S., and van Beuningen, D. (1974). Influence of NAD+ on development of mouse blastocysts in vitro. Nature *250*, 434–435.

Sturmey, R.G., Reis, A., Leese, H.J., and McEvoy, T.G. (2009). Role of fatty acids in energy provision during oocyte maturation and early embryo development. Reprod. Domest. Anim. *44* (suppl 3), 50–58.

Sullivan, L.B., Gui, D.Y., Hosios, A.M., Bush, L.N., Freinkman, E., and Vander Heiden, M.G. (2015). Supporting aspartate biosynthesis is an essential function of respiration in proliferating cells. Cell *162*, 552–563.

Sullivan, W.J., Mullen, P.J., Schmid, E.W., Flores, A., Momcilovic, M., Sharpley, M.S., Jelinek, D., Whiteley, A.E., Maxwell, M.B., Wilde, B.R., et al. (2018). Extracellular matrix remodeling regulates glucose metabolism through TXNIP destabilization. Cell *175*, 117–132.

Van Winkle, L.J. (2001). Amino acid transport regulation and early embryo development. Biol. Reprod. *64*, 1–12.

Vander Heiden, M.G., and DeBerardinis, R.J. (2017). Understanding the intersections between metabolism and cancer biology. Cell *168*, 657–669.

Veech, R.L., Todd King, M., Pawlosky, R., Kashiwaya, Y., Bradshaw, P.C., and Curtis, W. (2019). The "great" controlling nucleotide coenzymes. IUBMB Life *71*, 565–579.

White, M.D., Bissiere, S., Alvarez, Y.D., and Plachta, N. (2016). Mouse embryo compaction. Curr. Top. Dev. Biol. *120*, 235–258.

Williamson, D.H., Lund, P., and Krebs, H.A. (1967). The redox state of free nicotinamide-adenine dinucleotide in the cytoplasm and mitochondria of rat liver. Biochem. J. *103*, 514–527.

Xia, J., and Wishart, D.S. (2011). Web-based inference of biological patterns, functions and pathways from metabolomic data using MetaboAnalyst. Nat Protoc. *6*, 743–760.

Zhang, H., Badur, M.G., Divakaruni, A.S., Parker, S.J., Jäger, C., Hiller, K., Murphy, A.N., and Metallo, C.M. (2016). Distinct metabolic states can support self-renewal and lipogenesis in human pluripotent stem cells under different culture conditions. Cell Rep. *16*, 1536–1547.

STAR★METHODS

KEY RESOURCES TABLE

REAGENT or RESOURCE	SOURCE	IDENTIFIER
Antibodies		
Rabbit monoclonal anti-PKM2 (D78A4)	Cell Signaling	Cat #4053; RRID: AB_1904096
Goat polyclonalanti-PFK1	Santa Cruz	Cat #sc-31712; RRID: AB_2163022
Mouse monoclonal anti-GAPDH	Santa Cruz	Cat #sc-32233; RRID: AB_627679
Rabbit polyclonal to PDHE1a (phospho S293)	Abcam	Cat #ab92696; RRID: AB_10711672
Rabbit polyclonal to Glutaminase (GLS)	Abcam	Cat #ab93434; RRID: AB_10561964
Rabbit monoclonal [EPR11370] to GLUD1	Abcam	Cat #ab168352; RRID: AB_2889200
Rabbit polyclonal to c-Myc	Santa Cruz	Cat #sc-764; RRID: AB_631276
Chemicals, peptides, and recombinant proteins		
YZ9 (1μM)	Cayman Chemical	Cat #15352
KJ-Pyr-9 (20nM)	Cayman Chemical	Cat #19116
CB-839 (100nM)	Cayman Chemical	Cat #22038
O-(Carboxymethyl) hydroxylamine hemihydrochloride (AOA: 0.5mM)	Sigma-Aldrich	Cat #C13408
L-Methionine sulfoximine (MSO: 1mM)	Sigma-Aldrich	Cat #M5379
Etomoxir (5μM)	Sigma-Aldrich	Cat #E1905
UK-5099 (500nM)	Sigma-Aldrich	Cat #PZ0160
Sodium octanoate	Sigma-Aldrich	Cat #C5038-10G
U-$^{13}C_5$-L-Glutamine (1 mM)	Cambridge Isotope Laboratories	Cat #CLM-1822-H-0.1
U-$^{13}C_6$-D-Glucose (200μM)	Cambridge Isotope Laboratories	Cat #CLM-1396-PK
U-$^{13}C_3$-Pyruvic Acid Sodium Salt (200μM)	Cambridge Isotope Laboratories	Cat #CLM-2440-0.5
U-$^{13}C_3$-L-(+)-Lactic Acid Sodium Salt (5mM)	Cambridge Isotope Laboratories	Cat #CLM-10768-PK
U-$^{13}C_5$-alpha-ketoisovaleric acid sodium salt (1 mM)	Cambridge Isotope Laboratories	Cat #CLM-4418-0.25
U-$^{13}C_2$-glycine	Cambridge Isotope Laboratories	Cat #CLM-1017-0.5
U-$^{13}C_4$ L-aspartate acid	Cambridge Isotope Laboratories	Cat#CLM-1801-H-0.25
[1,2]$^{13}C_2$, D-glucose	Cambridge Isotope Laboratories	Cat#CLM-504-0.25
Pregnant Mare Serum Gonadotropin (PMSG)	ProSpec	Cat #hor-272
Chorionic gonadotropin human (hCG)	Sigma-Aldrich	Cat #CG10
α-Ketoisocaproic acid (KIC, 1mM)	Sigma-Aldrich	Cat #68255-1G
Sodium 3-methyl-2-oxobutyrate (KIV, 1 mM)	Sigma-Aldrich	Cat #198994-5G
Sodium α-ketobutyrate (KB, 1 mM)	Sigma-Aldrich	Cat #K0875-5G
α-Ketovaleric acid (KV, 1 mM)	Sigma-Aldrich	Cat #75950-5ML
2-Ketohexanoic acid sodium salt (KH, 1mM)	Sigma-Aldrich	Cat #K6625
β-Nicotinamide adenine dinucleotide, reduced disodium salt hydrate (NADH)	Sigma-Aldrich	Cat # N8129-100MG
β-Nicotinamide adenine dinucleotide (NAD^+)	Sigma-Aldrich	Cat # N8285-15VL
Nicotinamide	Sigma-Aldrich	Cat # N0636-100G
Nicotinic acid	Sigma-Aldrich	Cat # N0761-100G
β-Nicotinamide adenine dinucleotide 2′-phosphate reduced tetrasodium salt hydrate (NADPH)	Sigma-Aldrich	Cat # 10107824001
β-Nicotinamide adenine dinucleotide phosphate hydrate ($NADP^+$)	Sigma-Aldrich	Cat # N5755-100MG
Critical commercial assays		
NADH/NAD glo assay	Promega	Cat #G9071
Deposited data		
RNA-seq from embryos at 12 developmental time-points cultured using media with and without key nutrients	This study	GEO: GSE159484

(*Continued on next page*)

Continued

REAGENT or RESOURCE	SOURCE	IDENTIFIER
Experimental models: Cell lines		
Mouse: embryo culture	This lab	N/A
Experimental models: Organisms/Strains		
Mouse: B6C3F1/J	Jackson Laboratory	Stock No: 100010
Software and algorithms		
Graphpad Prism 7	GraphPad	http://www.graphpad.com/
ImageJ	NIH	https://imagej.nih.gov/ij/
MetaboAnalyst	(Xia and Wishart, 2011)	https://www.metaboanalyst.ca/
Partek software package	Partek Incopr.	https://www.partek.com/
Tracefinder	Thermo.	https://www.thermofisher.com
Imaris software package	Imaris	https://imaris.oxinst.com/

RESOURCE AVAILABILITY

Lead contact

Further information and requests for resources and reagents should be directed to and will be fulfilled by the lead contact, Mark Sharpley (Mark.Sharpley@cshs.org).

Materials availability

This study did not generate new unique reagents.

Data and code availability

- RNA-seq data have been deposited at GEO and are publicly available as of the date of publication. Accession numbers are listed in the key resources table. Microscopy data reported in this paper will be shared by the lead contact upon request.
- No original code was generated in this study.
- Any additional information required to reanalyze the data reported in this paper is available from the lead contact upon request.

EXPERIMENTAL MODEL AND SUBJECT DETAILS

Preimplantation mouse embryos

All animal care and procedures used in this study are approved by the Animal Regulatory Committee (ARC) of the University of California at Los Angeles (UCLA).

Mouse zygotes and preimplantation embryos were collected from super-ovulated 4-week old C57BL/6J X C3He (Jackson Labs) F1 females. Mice were super-ovulated by peritoneal injection of 7.5 IU of PMSG (Pregnant Mare Serum Gonadotropin) to stimulate egg production, followed by 7.5 IU of hCG (human Chorionic Gonadotropin) 48h after PMSG. Embryos were obtained by mating the super-ovulated females with C57BL/6 X C3He F1 males.

METHOD DETAILS

Reagents

The following antibodies and drugs were used in this study. Fluorescein Phalloidin (Thermo Fisher #F432, at 1:2000 dilution), rabbit anti-PKM2 (CST #4053), goat anti-PFK1 (Santa Cruz #sc-31712), mouse anti-GAPDH (Santa Cruz #sc-32233), rabbit anti-GLS (Abcam #ab93434), rabbit anti-GLUD1 (Abcam #ab168352), and rabbit anti-c-Myc (Santa Cruz #sc-764). All the antibodies are used at 1:100 dilution for IF. The chemical reagents used in this study were: YZ9 (Cayman Chemical #15352, 1μM), KJ-Pyr-9 (Cayman Chemical #19116, 20nM), CB-839 (Cayman Chemical #22038, 100nM), O-(Carboxymethyl)hydroxylamine hemihydrochloride (AOA) (Sigma #C13408, 0.5mM), L-Methionine sulfoximine (MSO) (Sigma #M5379, 1mM), Etomoxir (Sigma #E1905, 5μM), UK-5099 (Sigma # PZ0160, 500nM). The inhibitors were used at the time indicated in the text to treat groups of 30 embryos, with each treatment performed on several independent cohorts of embryos. To avoid absorption of inhibitors into the oil-overlay, hydrophobic inhibitors were provided to embryos that were cultured under oil-free conditions.

Embryo isolation and culture

For isolation of fertilized 1-cell zygotes, super-ovulated females were euthanized 18h post hCG and zygotes were dissected out of the ampulla in the oviduct. The embryo cumulus complexes were treated with 300μg/ml of hyaluronidase to disperse the cumulus cells,

washed in mKSOM medium without pyruvate/glucose and transferred to the appropriate culture medium and cultured at 37°C in 5% CO_2. All mouse embryos used in this study were cultured in a modified KSOM medium whose composition is identical to KSOM in salts, glucose, lactate and pyruvate (95mM NaCl, 2.5mM KCl, 0.35mM KH_2PO_4, 0.20mM $MgSO_4$, 25mM $NaHCO_3$, 1.71mM $CaCl_2$, 0.01 mM EDTA, 0.20mM glucose, 5mM L-lactate, 0.20mM pyruvate) but was devoid of all amino acids and BSA. The medium also contained 0.01% PVA (polyvinyl alcohol).

Antibody staining for immunofluorescence

Embryos were fixed in 4% paraformaldehyde for 30 min at room temperature, permeabilized for 30 min in PBS with 0.4% Triton (PBST), blocked in PBST with 3% albumin (PBSTA) for 30 min and incubated with the desired primary antibody in PBSTA overnight at 4°C. The following day the embryos were washed in PBST 4 times for 10 min each, blocked with PBSTA, incubated with the appropriate secondary antibody (1:500 dilution) and DAPI overnight at 4°C. Embryos were washed again 3 times for 10 min each in PBST, deposited on glass slides and mounted in Vectashield (Vector Laboratories) medium. Images were captured using Zeiss LSM700 or LSM880 confocal microscopes.

RNA sequencing experiments

The RNA-seq libraries were generated from early mouse embryos using the Smart-seq2 protocol as published with minor modification (Picelli et al., 2014). Cells were lysed in 0.1% (vol/vol) Triton X-100 lysis buffer containing 2.5μM of oligo-dT30VN primer, 2.5mM of dNTP mix and 1U/μl of RNase inhibitor. After 3 mins lysis at 72°C, the Smart-seq2 reverse transcription mixture was added for reverse transcription. After pre-amplification and AMPure XP beads purification, 0.5ng of cDNA was used for the Tn5 tagmentation reaction. Libraries were sequenced on Illumina HiSeq-4000 according to the manufacturer's instruction. The RNA sequencing data were analyzed using Partek software suite. The reads data were aligned to mouse reference genome mm10-ensembl transcripts (release 97) using the STAR package that is embedded in Partek.

Measurement of metabolite levels

The metabolites are measured using the procedure described previously (Nagaraj et al., 2017; Sullivan et al., 2018). For samples analyzed under different conditions, embryos were washed very briefly in ice-cold 150mM ammonium acetate (pH 7.3), and extracted with 80% methanol. Dried metabolites were re-suspended in 20 μl 50% ACN and 5 μl was injected onto a Luna 3mm NH2 100A (150 × 2.0mm) (Phenomenex) column. Chromatographic separation was performed on an UltiMate 3000 RSLC or a Vanquish Flex (Thermo Scientific) UHPLC system with mobile phases (A) 5mM NH4AcO, pH 9.9 and (B) ACN and a flowrate of 200 μL/min. An 18 min linear gradient from 15% A to 95% A was followed by a 9 min isocratic step at 95% A before re-equilibration to 15% A. Metabolites were detected with a Thermo Scientific Q Exactive mass spectrometer run with polarity switching in full SIM mode using a scan range of 65-975 m/z and resolution of 70K. The remainder of the sample was diluted 2.67-fold and 10μl was submitted to a Thermo Scientific Ion Chromatography System (ICS) 5000 for separation on a Dionex IonPac AS11-HC-4μm anion-exchange column using a flow rate of 350 μl/min and a 13 min gradient of 5-95 mM KOH. The Q Exactive acquired full SIM data in negative polarity mode at 70K resolution with a scan range of 70-900 m/z. Metabolites were identified based on accurate mass (±3 ppm) and retention times of pure standards. Relative amounts of metabolites and contribution of ^{13}C labeled nutrients (following correction for natural abundance) were quantified using TraceFinder 4.1 (Thermo Scientific). Values were normalized by embryo number. The data were analyzed using the Prism software package and the Metaboanalyst R package.

NAD^+ and NADH levels were determined using the NAD^+/NADH Glo cycling assay, according to the manufacturer's instructions (Promega, WI, USA). Briefly, both NAD^+ and NADH were extracted from the embryos in a carbonate buffered base solution containing 1% DTAB, 10 mM nicotinamide, 0.05% Triton X-100, pH 10.7. The embryos were freeze-thawed in liquid nitrogen and centrifuged through a filter with a 10kDa mW cut-off. Samples for NAD^+ determination were neutralized with 0.4 N HCl. Both NAD^+ and NADH samples were heated for 20 min at 60°C. The assay reagent was added to the samples, which were then incubated for 2h for cycling, after which the luminescence was determined. For the all samples for which pyruvate was absent, glucose (0.2 mM) and L-lactate (5 mM) was present in the medium. For the 1C samples lacking pyruvate, pyruvate was absent from the time of isolation (20h) and NAD(H) were measured 6h later (26h). For 2C, pyruvate was removed from the time of isolation (20h) and measured 26h later (46h). For the morula stage samples, pyruvate was removed at 52h (late 2C) and NAD(H) was measured at 78h. For the blastocyst stage, pyruvate was removed at 72h and NAD(H) measured at 98h.

Labeling conditions

$U^{13}C$ glucose labeling of 2C embryos, morula and blastocysts (see Figures 1C, 1I, 1K, S1B, S1E–S1G, and S1I)

The conditions described in this section are an example of the "**Standard Isotopologue Labeling Protocol**". For the 2C samples, embryos were isolated at the zygote stage (~22h post-hCG), and then placed into media containing 0.2 mM $U^{13}C$ D-glucose, 0.2 mM $U^{12}C$ pyruvate and 5 mM $U^{12}C$ L-lactate. No other nutrients, such as amino acids or BSA, were included in the media. After 26h of culture, metabolites were extracted at 48h.

For the morula stage samples, embryos were isolated at the zygote stage (~22h), and then placed into media containing 0.2 mM $U^{13}C$ D-glucose, 0.2 mM $U^{12}C$ pyruvate and 5 mM $U^{12}C$ L-lactate. No other nutrients, such as amino acids or BSA, were included in

the media. At 52h (late 2-cell stage) embryos were transferred into fresh media containing 0.2 mM U^{13}C D-glucose, 0.2 mM U^{12}C pyruvate and 5 mM U^{12}C L-lactate. Then, at the compacted 8-16C stage (78h) metabolites were extracted (26h following transfer into fresh media, 54h total exposure to ^{13}C glucose).

For the blastocyst samples, embryos were isolated at the zygote stage (~22h), and then placed into media containing 0.2 mM U^{13}C D-glucose, 0.2 mM U^{12}C pyruvate and 5 mM U^{12}C L-lactate. No other nutrients, such as amino acids or BSA, were included in the media. At 72h embryos were transferred to fresh media containing 0.2 mM U^{13}C D-glucose, 0.2 mM U^{12}C pyruvate and 5 mM U^{12}C L-lactate, and metabolites were extracted at 98h (26h following transfer into fresh media, 76h total exposure to ^{13}C glucose).

[1, 2]^{13}C glucose labeling of 2C embryos, morula and blastocysts (see Figures 1E and 1N)

For the 2C samples, embryos were isolated at the zygote stage (~22h), and then placed into media containing 0.2 mM [1, 2]^{13}C D-glucose, 0.2 mM U^{12}C pyruvate and 5 mM U^{12}C L-lactate. No other nutrients, such as amino acids or BSA, were included in the media. After 26h of culture, metabolites were extracted at 48h.

For the morula stage samples, embryos were isolated at the zygote stage (~22h), and then placed into media containing 0.2 mM [1, 2]^{13}C D-glucose, 0.2 mM U^{12}C pyruvate and 5 mM U^{12}C L-lactate. No other nutrients, such as amino acids or BSA, were included in the media. At 52h (late 2-cell stage) embryos were transferred into fresh media containing 0.2 mM [1, 2]^{13}C D-glucose, 0.2 mM U^{12}C pyruvate and 5 mM U^{12}C L-lactate. Then at the compacted 8-16C stage (78h) metabolites were extracted (26h following transfer into fresh media, 54h total exposure to ^{13}C glucose).

For the blastocyst samples subject to the Standard Isotopologue Labeling Protocol (labeled "B" in the figure) in which embryos were exposed to labeled glucose throughout, embryos were isolated at the zygote stage (~22h), and then placed into media containing 0.2 mM [1,2]^{13}C D-glucose, 0.2 mM U^{12}C pyruvate and 5 mM U^{12}C L-lactate. No other nutrients, such as amino acids or BSA, were included in the media. At 72 h embryos were transferred to fresh media containing 0.2 mM [1, 2]^{13}C D-glucose, 0.2 mM U^{12}C pyruvate and 5 mM U^{12}C L-lactate, and metabolites were extracted at 98h (26h following transfer into fresh media, 76h total exposure to ^{13}C glucose).

For the blastocyst samples subject to the "**Pulse Protocol**" (labeled "B^{pulse}" in the figure) in which embryos were exposed to labeled glucose for only 26h prior to metabolite extraction, embryos were isolated at the zygote stage (~22h), and then placed into media containing 0.2 mM ^{12}C D-glucose, 0.2 mM U^{12}C pyruvate and 5 mM U^{12}C L-lactate. No other nutrients, such as amino acids or BSA, were included in the media. At 72h embryos were transferred to fresh media containing 0.2 mM [1, 2]^{13}C D-glucose, 0.2 mM U^{12}C pyruvate and 5 mM U^{12}C L-lactate, and metabolites were extracted at 98h (26h following transfer into fresh media, 26h total exposure to ^{13}C glucose).

U^{13}C glucose labeling of morula stage embryos following a short incubation in labeled glucose at 1-2C (see Figure S1J)

For these morula stage samples glucose is only provided during the 1-2C stage. Embryos were isolated at the zygote stage (~22h), and then placed into media containing 0.2 mM U^{13}C D-glucose, 0.2 mM U^{12}C pyruvate and 5 mM U^{12}C L-lactate. No other nutrients, such as amino acids or BSA, were included in the media. At 52h (late 2-cell stage) embryos were transferred into fresh media containing no glucose, but with 0.2 mM U^{12}C pyruvate and 5 mM U^{12}C L-lactate. Then at the morula stage (78h) metabolites were extracted (26h following transfer into fresh media, 26h exposure to ^{13}C glucose in media at the 1-2C stage, followed by a 26h "chase" in no glucose media).

^{13}C glycine labeling of morula stage embryos (see Figure 1L)

Metabolites were extracted at the morula stage (78h). There were two conditions: 1) embryos that have access to glucose, 2) embryos that have not been provided with glucose. In both conditions, embryos were provided with 1mM U^{13}C glycine from the zygote stage. In detail, embryos were isolated at the zygote stage (~22h). Embryos to be exposed to glucose (PGL group), were placed into media containing 0.2 mM U^{12}C D-glucose, 0.2 mM U^{12}C pyruvate, 5 mM U^{12}C L-lactate and 1 mM U^{13}C glycine. The embryos that were not to be provided access to glucose (PL group) were placed into media containing 0.2 mM U^{12}C pyruvate, 5 mM U^{12}C L-lactate and 1 mM U^{13}C glycine. No other nutrients, such as amino acids or BSA, were included in the media. At 52h (late 2-cell stage) embryos were transferred into fresh media containing either (PGL group) 0.2 mM U^{12}C D-glucose, 0.2 mM U^{12}C pyruvate, 5 mM U^{12}C L-lactate and 1 mM U^{13}C glycine or (GL group) 0.2 mM U^{12}C pyruvate, 5 mM U^{12}C L-lactate and 1 mM U^{13}C glycine. Then at the morula stage (78h) metabolites were extracted (26h following transfer into fresh media, 54 h total exposure to ^{13}C glycine).

^{13}C pyruvate and lactate labeling of 2C embryos, morula and blastocysts (see Figures 2A, 2D, 2H, S2A, and S2C)

These embryos were subject to the Standard Isotopologue Labeling Protocol. For the 2C samples, embryos were isolated at the zygote stage (~22h), and then placed into media containing 0.2 mM U^{12}C D-glucose, 0.2 mM U^{13}C pyruvate and 5 mM U^{13}C L-lactate. Both pyruvate and lactate were labeled as these nutrients exchange extensively via the lactate dehydrogenase reaction. No other nutrients, such as amino acids or BSA, were included in the media. After 26h of culture, metabolites were extracted at 48h.

For the morula stage samples, embryos were isolated at the zygote stage (~22 h), and then placed into media containing 0.2 mM U^{12}C D-glucose, 0.2 mM U^{13}C pyruvate and 5 mM U^{13}C L-lactate. No other nutrients, such as amino acids or BSA, were included in the media. At 52h (late 2-cell stage) embryos were transferred into fresh media containing 0.2 mM U^{12}C D-glucose, 0.2 mM U^{13}C pyruvate and 5 mM U^{13}C L-lactate. Then at the morula stage (78h) metabolites were extracted (26h following transfer into fresh media, 54h total exposure to ^{13}C pyruvate/lactate).

For the blastocyst samples, embryos were isolated at the zygote stage (~22h), and then placed into media containing 0.2 mM U^{12}C D-glucose, 0.2 mM U^{13}C pyruvate and 5 mM U^{13}C L-lactate. No other nutrients, such as amino acids or BSA, were included in the media. At 72h embryos were transferred to fresh media containing 0.2 mM U^{12}C D-glucose, 0.2 mM U^{13}C pyruvate and 5 mM U^{13}C L-lactate, and metabolites were extracted at 98h (26h following transfer into fresh media, 76h total exposure to ^{13}C pyruvate/lactate).

^{13}C glutamine labeling of 2C embryos, morula and blastocysts (see Figures 2J, S2E, and S2F)

For the 2C samples, embryos were isolated at the zygote stage (~22h), and then placed into media containing 0.2 mM U^{12}C D-glucose, 0.2 mM U^{12}C pyruvate, 5 mM U^{12}C L-lactate and 1 mM U^{13}C glutamine. No other nutrients, such as amino acids or BSA, were included in the media. After 26h of culture, metabolites were extracted at 48h.

For the morula stage samples, embryos were isolated at the zygote stage (~22h), and then placed into media containing 0.2 mM U^{12}C D-glucose, 0.2 mM U^{12}C pyruvate, 5 mM U^{12}C L-lactate and 1 mM U^{13}C glutamine. No other nutrients, such as amino acids or BSA, were included in the media. At 52h (late 2-cell stage) embryos were transferred into fresh media containing 0.2 mM U^{12}C D-glucose, 0.2 mM U^{12}C pyruvate, 5 mM U^{12}C L-lactate and 1 mM U^{13}C glutamine. Then at the morula stage (78h) metabolites were extracted (26h following transfer into fresh media, 54h total exposure to ^{13}C glutamine).

For the blastocyst samples, embryos were isolated at the zygote stage (~22h), and then placed into media containing 0.2 mM U^{12}C D-glucose, 0.2 mM U^{12}C pyruvate, 5 mM U^{12}C L-lactate and U^{13}C glutamine. No other nutrients, such as amino acids or BSA, were included in the media. At 72 h embryos were transferred to fresh media containing 0.2 mM U^{12}C D-glucose, 0.2 mM U^{12}C pyruvate, 5 mM U^{12}C L-lactate and 1 mM U^{13}C glutamine, and metabolites were extracted at 98h (26h following transfer into fresh media, 76h total exposure to ^{13}C glutamine).

^{13}C pyruvate and ^{13}C lactate labeling of 2C embryos with unlabeled glutamine present or absent (see Figure 2K)

For the 2C samples, embryos were isolated at the zygote stage (~22h), and then placed into media that either contained (+Gln group) 0.2 mM U^{12}C D-glucose, 0.2 mM U^{13}C pyruvate, 5 mM U^{13}C L-lactate and 1 mM U^{12}C glutamine or (- Gln group) 0.2 mM U^{12}C D-glucose, 0.2 mM U^{13}C pyruvate, and 5 mM U^{13}C L-lactate. Both pyruvate and lactate were labeled as these nutrients exchange extensively via the lactate dehydrogenase reaction. No other nutrients, such as additional amino acids or BSA, were included in the media. After 26h of culture, metabolites were extracted at 48h.

^{13}C aspartate labeling of 2C embryos, morula and blastocysts (see Figures 2J, S2I, and S2J)

For the 2C samples, embryos were isolated at the zygote stage (~22h), and then placed into media containing 0.2 mM U^{12}C D-glucose, 0.2 mM U^{12}C pyruvate, 5 mM U^{12}C L-lactate and 1 mM U^{13}C aspartate. No other nutrients, such as amino acids or BSA, were included in the media. After 26h of culture, metabolites were extracted at 48h.

For the morula stage samples, embryos were isolated at the zygote stage (~22h), and then placed into media containing 0.2 mM U^{12}C D-glucose, 0.2 mM U^{12}C pyruvate, 5 mM U^{12}C L-lactate and 1 mM U^{13}C aspartate. No other nutrients, such as amino acids or BSA, were included in the media. At 52h (late 2-cell stage) embryos were transferred into fresh media containing 0.2 mM U^{12}C D-glucose (unless otherwise stated), 0.2 mM U^{12}C pyruvate, 5 mM U^{12}C L-lactate and 1 mM U^{13}C aspartate. Then at the morula stage (78h) metabolites were extracted (26h following transfer into fresh media, 54h total exposure to ^{13}C Asp).

For the Standard Isotopologue Labeling Protocol blastocyst samples (Figure 2J), embryos were isolated at the zygote stage (~22h), and then placed into media containing 0.2 mM U^{12}C D-glucose, 0.2 mM U^{12}C pyruvate, 5 mM U^{12}C L-lactate and 1 mM U^{13}C aspartate. No other nutrients, such as amino acids or BSA, were included in the media. At 72h embryos were transferred to fresh media containing 0.2 mM U^{12}C D-glucose, 0.2 mM U^{12}C pyruvate, 5 mM U^{12}C L-lactate and 1 mM U^{13}C aspartate, and metabolites were then extracted at 98h (26h following transfer into fresh media, 76h total exposure to ^{13}C Asp).

For blastocyst samples studied using the Pulse Protocol (Figure S2J), embryos were isolated at the zygote stage (~22h), and then placed into media containing 0.2 mM U^{12}C D-glucose, 0.2 mM U^{12}C pyruvate, and 5 mM U^{12}C L-lactate (i.e., Asp-free medium). No other nutrients, such as amino acids or BSA, were included in the media. At 72h embryos were transferred to fresh media containing 0.2 mM U^{12}C D-glucose, 0.2 mM U^{12}C pyruvate, 5 mM U^{12}C L-lactate and 1 mM U^{13}C aspartate, and metabolites were extracted at 98h (26h following transfer into fresh media, 26h total exposure to ^{13}C Asp).

^{13}C lactate +/- ^{13}C pyruvate labeling of 2C embryos (see Figures 3B, 3C, 3F, and S3D)

Embryos were isolated at the zygote stage (~22h), and then placed into media that either contained (PGL group) 0.2 mM U^{12}C D-glucose, 0.2 mM U^{13}C pyruvate, 5 mM U^{13}C L-lactate or (GL group) 0.2 mM U^{12}C D-glucose and 5 mM U^{13}C L-lactate (i.e., pyruvate-free media). When present, both pyruvate and lactate were labeled as these nutrients exchange extensively via the lactate dehydrogenase reaction. No other nutrients, such as additional amino acids or BSA, were included in the media. After 26h of culture, metabolites were extracted at 48h.

^{13}C lactate +/- ^{13}C pyruvate labeling of morula stage embryos (see Figures 3C′, 3G, and S3D′)

Embryos were isolated at the zygote stage (~22h), and then placed into media containing 0.2 mM U^{12}C D-glucose, 0.2 mM U^{13}C pyruvate and 5 mM U^{13}C L-lactate. No other nutrients, such as amino acids or BSA, were included in the media. At 52 h (late 2-cell stage) embryos were transferred into fresh media that either contained (PGL group) 0.2 mM U^{12}C D-glucose, 0.2 mM U^{13}C pyruvate and 5 mM U^{13}C L-lactate or (GL group) 0.2 mM U^{12}C D-glucose and 5 mM U^{13}C L-lactate (i.e., pyruvate-free media). Then at the morula stage (78h) metabolites were extracted (26h following transfer into fresh media, 54h total exposure to ^{13}C lactate +/- pyruvate).

^{13}C glucose labeling of 2C embryos with pyruvate absent (see Figure 3D)

Embryos were isolated at the zygote stage (~22h), and then placed into media that contained 0.2 mM U^{13}C D-glucose and 5 mM U^{12}C L-lactate. No other nutrients, such as additional amino acids or BSA, were included in the media. After 26h of culture, metabolites were extracted at 48h.

^{13}C glucose labeling of morula stage embryos with pyruvate present or absent (see Figures 3C′ and 3G)

Embryos were isolated at the zygote stage (~22h), and then placed into media containing 0.2 mM (or 10 mM) U^{13}C D-glucose, 0.2 mM U^{12}C pyruvate and 5 mM U^{12}C L-lactate. No other nutrients, such as amino acids or BSA, were included in the media. At

52h (late 2-cell stage) embryos were transferred into fresh media that either contained (PGL group) 0.2 mM (or 10 mM) $U^{13}C$ D-glucose, 0.2 mM $U^{12}C$ pyruvate and 5 mM $U^{12}C$ L-lactate or (GL group) 0.2 mM (or 10 mM) $U^{13}C$ D-glucose and 5 mM $U^{12}C$ L-lactate. Then at the morula stage (78h) metabolites were extracted.

^{13}C pyruvate and lactate labeling of morula stage embryos with pyruvate or lactate present or absent (see Figures 4D and 4D′)

Embryos were isolated at the zygote stage (~22h), and then placed into media containing 0.2 mM $U^{12}C$ D-glucose, 0.2 mM $U^{13}C$ pyruvate and 5 mM $U^{13}C$ L-lactate. No other nutrients, such as amino acids or BSA, were included in the media. At 52h (late 2-cell stage) embryos were transferred into fresh media that either contained (PGL group) 0.2 mM $U^{12}C$ D-glucose, 0.2 mM $U^{13}C$ pyruvate and 5 mM $U^{13}C$ L-lactate or (GL group) 0.2 mM $U^{12}C$ D-glucose and 5 mM $U^{13}C$ L-lactate or (PG group) 0.2 mM $U^{12}C$ D-glucose and 0.2 mM $U^{13}C$ pyruvate. Then at the morula stage (78h) metabolites were extracted.

^{13}C lactate labeling of 2C embryos with ^{13}C pyruvate present, absent or absent with a ketoacid or NAD$^+$ provided (see Figures 4L, 4M, 4P, 4P′, 4S, and S4M–S4O)

Embryos were isolated at the zygote stage (~22h), and then placed into media that either contained (PGL group) 0.2 mM $U^{12}C$ D-glucose, 0.2 mM $U^{13}C$ pyruvate, 5 mM $U^{13}C$ L-lactate, or (GL group) 0.2 mM $U^{12}C$ D-glucose and 5 mM $U^{13}C$ L-lactate, or (GL, KIV group), 0.2 mM $U^{12}C$ D-glucose, 5 mM $U^{13}C$ L-lactate and 1 mM $U^{12}C$ alpha-ketoisovaleric acid (KIV), or (GL, NAD group) 0.2 mM $U^{12}C$ D-glucose, 5 mM $U^{13}C$ L-lactate and 5 mM $U^{12}C$ NAD^+. When present, both pyruvate and lactate were labeled as these nutrients exchange extensively via the lactate dehydrogenase reaction. No other nutrients, such as additional amino acids or BSA, were included in the media. After 26h of culture, metabolites were extracted at 48h.

^{13}C KIV labeling of 2C embryos in pyruvate-free media (see Figure 4T)

Embryos were isolated at the zygote stage (~22h), and then placed into media that contained 0.2 mM $U^{12}C$ D-glucose, 5 mM $U^{12}C$ L-lactate and 1 mM $U^{13}C$ alpha-ketoisovaleric acid (KIV). No other nutrients, such as additional amino acids or BSA, were included in the media. After 26h of culture, metabolites were extracted at 48h.

^{13}C glucose labeling of morula stage embryos with pyruvate present or absent or with both pyruvate and lactate absent with a ketoacid provided (see Figures 5A–5E′)

Embryos were isolated at the zygote stage (~22h), and then placed into media containing 0.2 mM $U^{13}C$ D-glucose, 0.2 mM $U^{12}C$ pyruvate and 5 mM $U^{12}C$ L-lactate. No other nutrients, such as amino acids or BSA, were included in the media. At 52h (late 2-cell stage) embryos were transferred into fresh media that either contained (PGL group) 10 mM $U^{13}C$ D-glucose, 0.2 mM $U^{12}C$ pyruvate and 5 mM $U^{12}C$ L-lactate, or (GL group) 10 mM $U^{13}C$ D-glucose and 5 mM $U^{12}C$ L-lactate or (G, KB group) 10 mM $U^{13}C$ D-glucose and 1 mM $U^{12}C$ alpha-ketobutyrate (KB). Then at the morula stage (78h) metabolites were extracted.

^{13}C glutamine labeling of morula stage embryos +/- pyruvate, lactate or an α-ketoacid (see Figure S5B)

Embryos were isolated at the zygote stage (~22h), and then placed into media containing 0.2 mM $U^{12}C$ D-glucose, 0.2 mM $U^{12}C$ pyruvate, 5 mM $U^{12}C$ L-lactate and 1 mM $U^{13}C$ glutamine. No other nutrients, such as amino acids or BSA, were included in the media. At 52h (late 2-cell stage) embryos were transferred into fresh media containing either (PGL group) 0.2 mM $U^{12}C$ D-glucose, 0.2 mM $U^{12}C$ pyruvate, 5 mM $U^{12}C$ L-lactate and 1 mM $U^{13}C$ glutamine, or (GL group) 0.2 mM $U^{12}C$ D-glucose, 5 mM $U^{12}C$ L-lactate and 1 mM $U^{13}C$ glutamine, or (PG group) 0.2 mM $U^{12}C$ D-glucose, 0.2 mM $U^{12}C$ pyruvate, and 1 mM $U^{13}C$ glutamine, or (PG, KB group) 0.2 mM $U^{12}C$ D-glucose, 0.2 mM $U^{12}C$ pyruvate, 1 mM alpha-ketobutyrate (KB) and 1 mM $U^{13}C$ glutamine, or (10G, KB) 10 mM $U^{12}C$ D-glucose, 1 mM KB, and 1 mM $U^{13}C$ glutamine. Then at the morula stage (78 h) metabolites were extracted (26h following transfer into fresh media, 54h total exposure to ^{13}C glutamine).

QUANTIFICATION AND STATISTICAL ANALYSIS

Statistical parameters are reported in the figure legends. Data is considered significant if $p < 0.05$. Statistical analysis was performed using GraphPad Prism software. ImageJ and the Imaris Software package were used to analyze confocal imaging data. The Metaboanalyst R package was used for analysis of metabolomic data, with metabolites highlighted in volcano plots if $P < 0.05$ and the $\log_2$ fold-change > +/-1.5. Analysis of RNA-seq data was performed using the Partek package, with heatmaps generated using GraphPad Prism software.